SINGLE-EVENT KINETIC MODELING OF THE HYDROCRACKING OF HYDROGENATED VACUUM GAS OIL

A Thesis

by

ALPER T. ERTAS

Submittal to the Office of Graduate Studies of
Texas A&M University
in partial fulfillment of the requirements for the degree of

MASTER OF SCIENCE

August 2005

Major Subject: Chemical Engineering

SINGLE-EVENT KINETIC MODELING OF THE HYDROCRACKING OF HYDROGENATED VACUUM GAS OIL

A Thesis

by

ALPER T. ERTAS

Submittal to the Office of Graduate Studies of
Texas A&M University
in partial fulfillment of the requirements for the degree of

MASTER OF SCIENCE

Approved By:

Chair of Committee,	Gilbert F. Froment
Committee Members,	Drago B. Bukur
	Wayne D. Goodman
Head of Department	Kenneth R. Hall

August 2005

Major Subject: Chemical Engineering

ABSTRACT

Single-Event Kinetic Modeling of the Hydrocracking of Hydrogenated Vacuum Gas Oil. (August 2005)

Alper T. Ertas B.S., Texas A&M University

Chair of Advisory Committee: Dr. Gilbert F. Froment

The primary objective of the research project was to further develop a computer program modeling the hydrocracking of partially hydrogenated vacuum gas oil (HVGO), and to use the model to compare the theoretical product distribution to experimental data describing the product distribution of an industrial pilot reactor. The hydrocracking of HVGO on acid zeolites is effectively modeled utilizing a single-event kinetic approach developed by Froment and coworkers. The hydrocracking of HVGO can be described in terms of the fundamental reaction steps involving carbenium ions. Some 45 single-event rate parameters are used to dictate the rate of each single-event in the reaction network. The composition of the partially hydrogenated feed stock is detailed up to C_{33}. Each component and lump is considered in terms of the elementary steps to generate a network of continuity equations and single-event rate parameters. A reactor model comprising this kinetic model can be used to simulate the isothermal and non-isothermal hydrocracking of a HVGO feed stock. The results are represented in terms of the yields of 241 lumps and components in the gas phase and 241 components and lumps in the liquid phase. The predicted yields of various commercial oil fractions and particular components are then compared to experimental data from an industrial pilot reactor to verify the accuracy of the model and the single-event rate parameters.

ACKNOWLEDGEMENTS

I acknowledge Dr. Gilbert F. Froment for his commitment to furthering the field of chemical engineering and specifically his efforts in the modeling of complex processes. His guidance and past research has made this project possible.

I thank my committee members, Dr. Rayford G. Anthony, Dr. Drago B. Bukur, Dr. Wayne D. Goodman, and Dr. David E. Bergbreiter, for their instruction and aid during my graduate and undergraduate studies at Texas A&M University.

Finally, I thank my parents and brother Dr. Atila Ertas, Mrs. Necibe Ertas, and Dr. Bugra H. Ertas, for the constant support, love, and guidance throughout my life and especially during my undergraduate and graduate studies.

TABLE OF CONTENTS

Page

LIST OF FIGURES

Page

LIST OF TABLES

Page

CHAPTER I
INTRODUCTION

1.1 Background

The petroleum refining industry encounters many stringent environmental and market demands for cleaner and more purified fractions of fuels. Hydrocracking and hydroisomerization of hydrocarbons are among the most important basic processes in the petroleum process industry used to convert heavy fractions of crude oil into a broad range of highly valuable fractions of fuel. The process of hydrocracking encountered rapid growth between 1960 and 1970 with an increase from 1000 bbl/day in 1960 to 770,000 bbl/day in 1970 (Strangeland, 1974). This rapid growth is attributed to the versatility of the hydrocracking process step and its capability of desulfurizing vacuum residua, making lubricating oils, demetalizing catalytic cracker feed, cracking gas oils to jet fuel and gasoline, and cracking naphtha to LPG.

Although there are several benefits to hydrocracking including improved octane ratings for gasoline fractions, high product ratios of isobutene/n-butane in the butane fraction, and the variability of ratios of gasoline/distillate in the product stream, hydrocracking is best suited for the production of high quality middle distillates (Gary and Handwerk, 1984). Feed stocks that are resistant to catalytic cracking such as heavy aromatic cycle oils and coker distillates are commonly processed as feed streams in industrial hydrocrackers. These heavy aromatic oils are susceptible to cracking only when exposed to high partial pressures of hydrogen, high operating temperature, and high pressure.

The development of a reliable kinetic model that can accurately simulate reactions and predict product distributions of the hydrocracking process is very challenging, but also very practical from a commercial point of view. Currently, because of the large number of compounds present in typical feed stocks of industrial hydrocrackers, and because of a deficiency in the analytical methods used in industry to determine the feed composition, most kinetic models use a drastic simplification of the kinetics involved in the process by grouping large numbers of components into lumps. The particular lumps are designated by a specific

This thesis follows the style and format of *Chemical Engineering Science*.

boiling point range, and the predicted rate parameters are dependent on feed stock composition, disproportionately increasing as the number of lumps increases (Martens et al., 2001). A model that comprises a manageable set of fundamental rate parameters requires a translation of carbenium ion chemistry into an appropriate set of rate equations. A so-called single-event model developed by Baltanas et al (1989) employs a translation of carbenium ion chemistry into an appropriate set of rate equations by detailing the hydrocracking process into its most elementary steps, and derives rate equations containing kinetic parameters that are not dependent on composition. The latter of the two models is used to conduct the current research, and to predict the product distribution and fundamental kinetic parameters of an industrial hydrocracker.

1.2 Hydrocracking Process

Hydrocracking is a two-stage process combining catalytic cracking and hydrogenation, wherein heavier feedstocks are cracked in the presence of hydrogen to produce more desirable products. The process employs high pressure, high temperature, a catalyst, and hydrogen. Typical, commercial hydrocrackers operate at the following conditions (Scherzer and Gruia, 1996):

Catalyst Temperature	300-450^{o} C
Pressure	85-200 bars
Liquid Hourly Space Velocity	0.5-2.5 hr $^{-1}$
H_2/HC ratio	3,000-10,000 SCFB
H_2 Consumption	1,200-3,500 SCFB

Hydrocracking is used for feedstock that are difficult to process by either catalytic cracking or reforming, since these feedstocks are characterized usually by a high polycyclic aromatic content and/or high concentrations of the two principal catalyst poisons, sulfur and nitrogen compounds. The hydrocracking process largely depends on the nature of the feedstock and the relative rates of the two competing reactions, hydrogenation and cracking. When the feedstock has a high paraffinic content, the primary function of hydrogen is to prevent the formation of polycyclic aromatic compounds, called coke. Hydrogenation also serves to convert sulfur and nitrogen compounds present in the feedstock to hydrogen sulfide and ammonia.

In a typical two stage hydrocracking unit, preheated feedstock is mixed with recycled hydrogen and sent to the first-stage reactor, where catalysts convert sulfur and nitrogen compounds to hydrogen sulfide and ammonia. In this stage limited hydrocracking occurs. After the hydrocarbon mixture leaves the first stage, it is cooled and liquefied and run through a hydrocarbon separator. The hydrogen is recycled to the feedstock and the liquid is charged to a fractionator. Depending on the desired products and product specifications the fractionator is run to eliminate particular components from the first stage reactor out-turn. Kerosene-range material can be taken as a separate side-draw product or included in the fractionator bottoms with the gas oil. The fractionator bottoms are again mixed with a hydrogen stream and charged to the second stage. Since this material has already been subjected to some hydrogenation, cracking, and reforming in the first stage, the operations of the second stage are more severe (higher temperatures and pressures). Like the outturn of the first stage, the second stage product is separated from the hydrogen and charged to the fractionator. The flow diagram of a typical hydrocracking unit is depicted in Fig. 1.1.

Safety considerations are vital when operating an industrial hydrocracking process; because this unit operates at very high pressures and temperatures, control of both hydrocarbon leaks and hydrogen releases is important to prevent fires and exposure to hydrocarbon gas, vapor emissions, and hydrogen sulfide gas. In some processes, care is needed to ensure that explosive concentrations of catalytic dust do not form during recharging. Inspection and testing of safety relief devices are important due to the very high pressures in this unit. Proper process control is needed to protect against plugging reactor beds. Unloading coked catalyst requires special precautions to prevent iron sulfide-induced fires and large quantities of carbon monoxide may be released during catalyst regeneration and changeover. The coked catalyst should either be cooled to below 50° C before dumping, or be placed in nitrogen-inerted containers until cooled. Several other precautions must be considered when operating an industrial hydocracking unit and safety should always be a primary consideration when efficiently operating commercial refining processes.

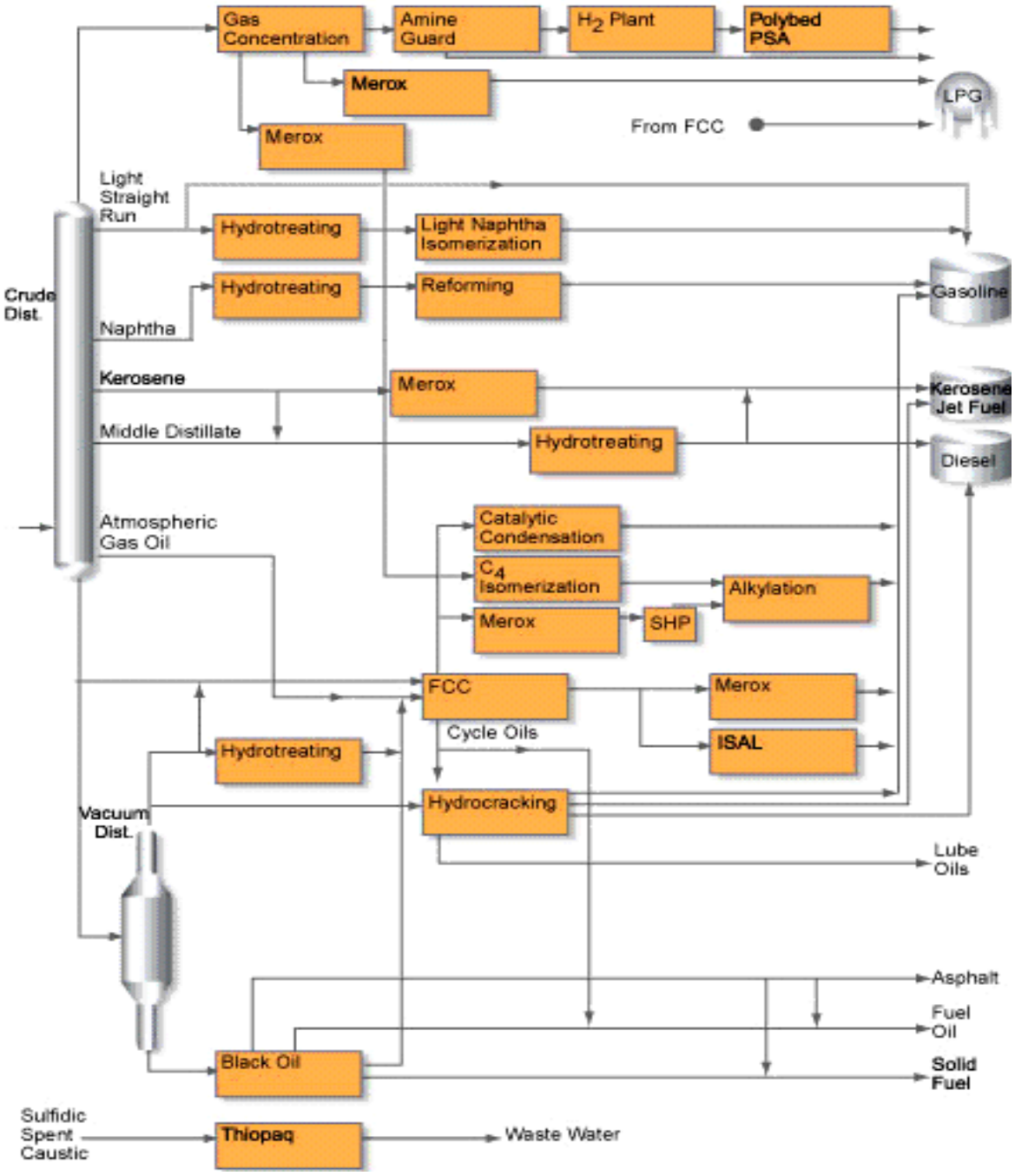

Fig. 1.1 Schematic of a Two-Stage Hydrocracking Unit (www.uop.com/refining/1010.html)

1.3 Literature Review

Development of an accurate kinetic model describing the hydrocracking process can provide a wealth of valuable information concerning the yields of industrial hydrocrackers. With an accurate kinetic model, countless expensive experiments in pilot plants can be avoided, by use of a computer algorithm. Furthermore, if the feedstock or operating conditions used in the process are altered the ability remains for the fundamental model to efficiently predict product distributions, without conducting laboratory experiments. The full potential of the fundamental model is realized when the operating conditions of the process are optimized to provide product distributions which are high in demand in the refining industry. In order to predict product distributions of an industrial hydrocracker and to obtain kinetic parameters that are independent of feed stock composition, the process must be described through its fundamental chemical steps.

There are various approaches currently prevalent in the literature employed to model the kinetics of the hydrocracking of vacuum gas oils (VGO), or residues. The current models used to simulate the hydrocracking of VGO can be placed into two distinct classes: lumped empirical models and detailed molecular models (Schweitzer, et al, 1999). Originally the most common approach to predicting hydrocracker yields was to select a small range of products and to devise parallel and series reactions that produce the selected products (Strangeland, 1974). Strangeland discusses a kinetic model used to predict hydrocracker yields, in which the feed and product streams are assumed to contain a continuum of compounds that can be characterized purely by boiling point. These compounds are then arranged into fixed boiling point ranges of 50^{o} F. Each compound undergoes a first order reaction to produce a spectrum of lighter products, and polymerization reactions that would produce heavier compounds are assumed to be negligible. Laximinarasimhan et al (1996) also devised a model representing the complex chemistry of hydrocracking by a continuous lumping approach. The true boiling point of the mixture is used as the characterization parameter. Since the rate constant of hydrocracking is assumed to be a monotonic function of the true boiling point, it is possible to reformulate mass-balance equations in terms of rate constant as a continuous variable. A distribution function $p(k, K)$, which determines the fractional yield distribution of species, was formulated based on data from the cracking patterns of various model compounds. Krishna and Saxena (1989) took a fundamentally different approach from earlier published models by use of the distribution of

boiling points around a mid-boiling temperature T_{50}, which after scaling can adequately be described by an axial dispersion model. To gain chemical insight on the axial dispersion parameter P_e and the decay kinetics at T_{50}, a detailed kinetic model is also developed using lumped paraffin, naphthene, aromatic, and sulfur species. The axial dispersion parameter, the mid-boiling temperature, and the selectivity of the catalyst are heavily governed by the paraffinicity of the entering feed stock.

Thus far, the techniques described used to model the hydrocracking of heavy petroleum fractions employ a reduced network of reactions between groups of molecules called lumps that are defined by their boiling point ranges. The deficiency associated with the lumped empirical model is that the rate parameters are a function of feed composition, and in order to obtain the product distribution the number of rate parameters increases to an unrealistic level as the number of lumps increases. Furthermore, the product distributions obtained from lumped empirical models are generally not very accurate. A single-event kinetic approach developed by Vynckier and Froment (1991), and coworkers at the 'Laboratorium voor Petrochemische Techniek" in Gent is employed to overcome the limitations that arise from the lumped empirical models. The single-event kinetic approach uses a computer algorithm developed by Baltanas and Froment (1985) which generates the complete reaction network, taking into account all the elementary steps that each molecule or carbocation undergoes during the hydrocracking process. The single-event kinetic approach involves describing the feed composition in terms of mole fraction or weight fraction, not in terms of physical properties, and all possible molecules pertaining to a lump are considered in the reaction network generation. The reactions involved in the hydrocracking network are expressed in terms of the fundamental elementary steps in carbenium ion chemistry. Through the employment of the single-event kinetic approach when modeling the hydrocracking of a VGO the rate parameters become independent of feed stock composition, and allow for efficient and accurate predictions of product distribution even though feed stocks and operating conditions are continually changing in the industry.

CHAPTER II
THEORY

2.1 Carbenium Ion and Zeolite Chemistry

Hydrocracking over a dual function metal/acid zeolite catalyst is an interesting option to produce high quality middle distillates. The acid components of bifunctional catalysts can include zeolites, zeolite-like solid acids, and acidic oxides. Decationized Y and mordenite zeolites are most widely applied in the hydrocracking of hydrocarbons, due to their strong acidic properties and specific pore geometry which allows for the reduction of pore diffusional resistances. Acting as the site of hydrogenation/dehydrogenation Pt, Pd, Ni, Co, and Mo, is commercially used as metal components of bifunctional catalysts. Metallic platinum is the most active metallic component used in catalysts, and as few as 0.2-0.5 wt% is required to promote the activity of (de)hydrogenation (Kuznetsov, 2003). Zeolites are alumina-silicates in which aluminum and silicon atoms are tetrahedrally coordinated to a set of four oxygen atoms. The geometric configuration is a set of rings composed of alternating silicon and oxygen atoms. The arrangement of rings gives rise to pores and cages seen in Fig. 2.1. The pores and cages formed in zeolites avoid to a certain degree, the deactivation of the catalyst from the polymerization of alkenes, which is sterically hindered from reacting in the molecular size pores of zeolites.

The complex chemistry involved in the hydrocracking of HVGO can be described through the elementary steps of carbenium ion chemistry which in this study, include such steps as, alkylation, dealkylation, disproportionation, cyclization, hydrogenation, dehydrogenation, isomerization, ring opening, paring, and cracking. For the task of modeling the hydrocracking of HVGO, to obtain a manageable set of rate parameters requires judicially translating carbenium ion chemistry into appropriate rate expressions.

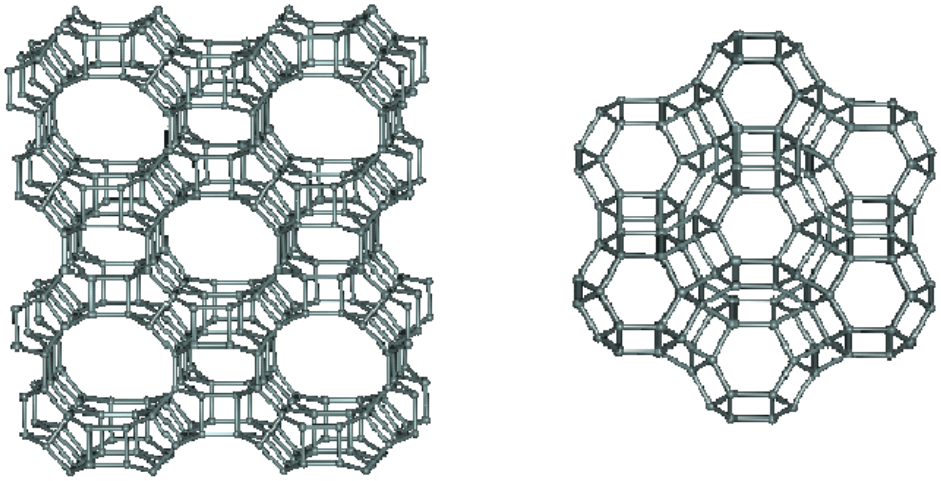

(a) (b)

Fig. 2.1. Zeolite Structures. (a) Mordenite (b) Fuajasite (Gauw, 2002)

HVGO feed stock contains paraffinic, naphthenic, aromatic, and naphtheno-aromatic feed components, and Figs. 2.2 and 2.3 represent the elementary steps for the hydrocracking of paraffinic components. After adsorption of a paraffinic species in the zeolite cage, the paraffins are dehydrogenated on the metal component of the hydrocracking catalyst to produce olefin intermediates. The olefins are then rapidly protonated on Bronsted acid sites yielding alkyl carbenium ions.

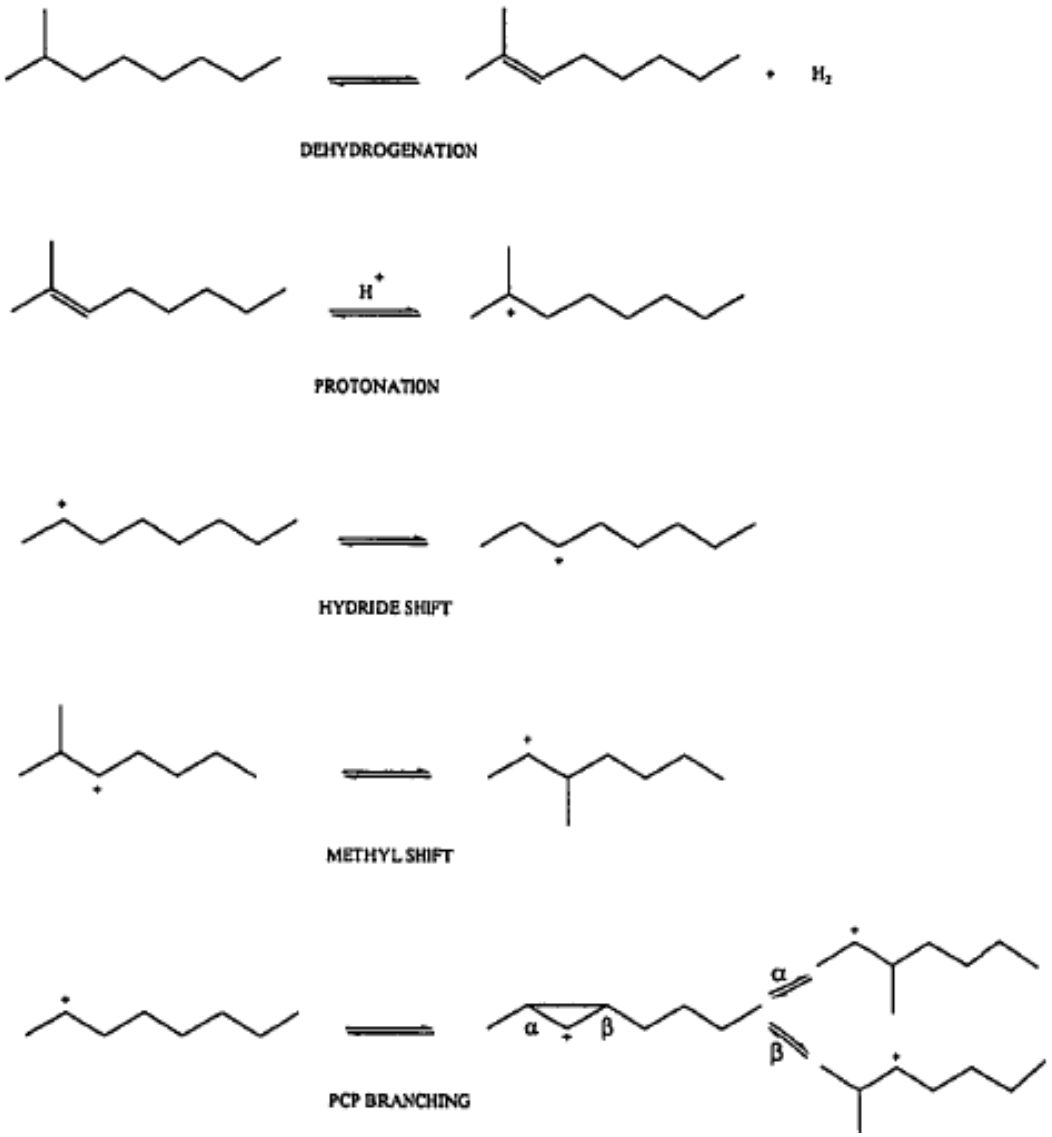

Fig. 2.2. Elementary Steps of Paraffin Isomerization (Alwahabi and Froment, 2004)

Isomerization of the alkyl carbenium ions occurs through hydride shift, methyl shift, and protonated cyclo propane (PCP) steps. The PCP steps create a higher degree of branching, making the molecule more susceptible to cracking at the C-C bond in the β-position with respect to the carbon atom bearing the positive charge. The product of β–scission is an olefin and a smaller carbenium ion. The former can protonate to yield another carbenium ion, or hydrogenate at the metal site of the catalyst to form paraffins. The carbenium ion formed from the β-scission step can further crack or deprotonate at the acid site to form a new olefin. The possibility of

either of the β-scission products undergoing protonation or hydrogenation depends on the relative strength of the acid/metal contributions of the dual functional catalyst.

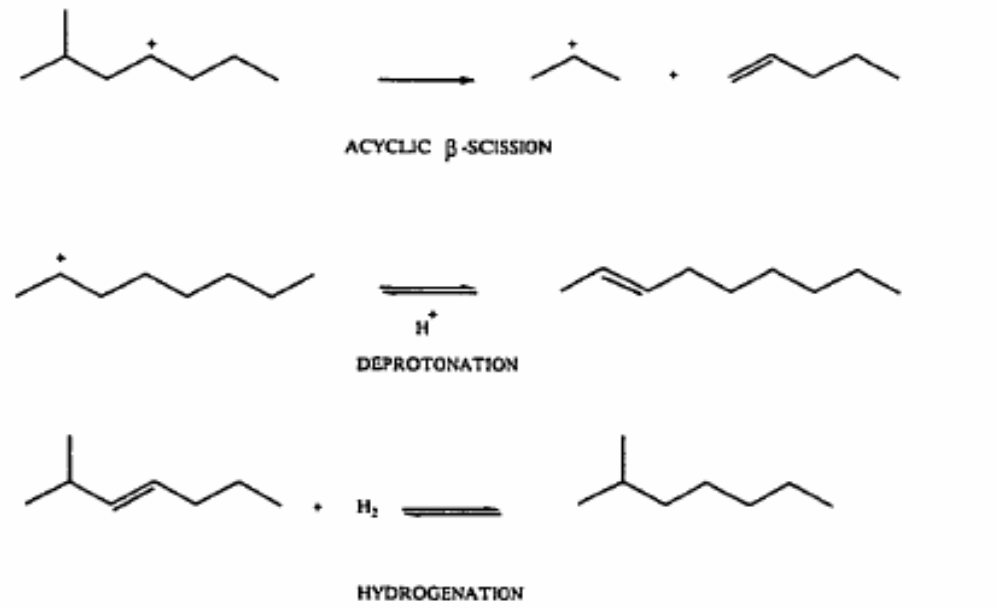

Fig. 2.3. Elementary Steps of Paraffin Cracking (Alwahabi and Froment, 2004)

The hydroisomerization reactions of naphthenic components of the HVGO are shown in Figs 2.4-2.7. Dehydrogenation of naphthenes occurs on the metal sites of the catalyst, and results in the formation of cyclic mono-olefins, which are protonated to cyclic carbenium ions. Isomerization of cyclic carbenium ions occurs through hydride shift, methyl shift, and PCP branching. The degree of branching of naphthenes is not altered by hydride and methyl shifts, but methyl shift does alter the relative position of substituents on the ring.

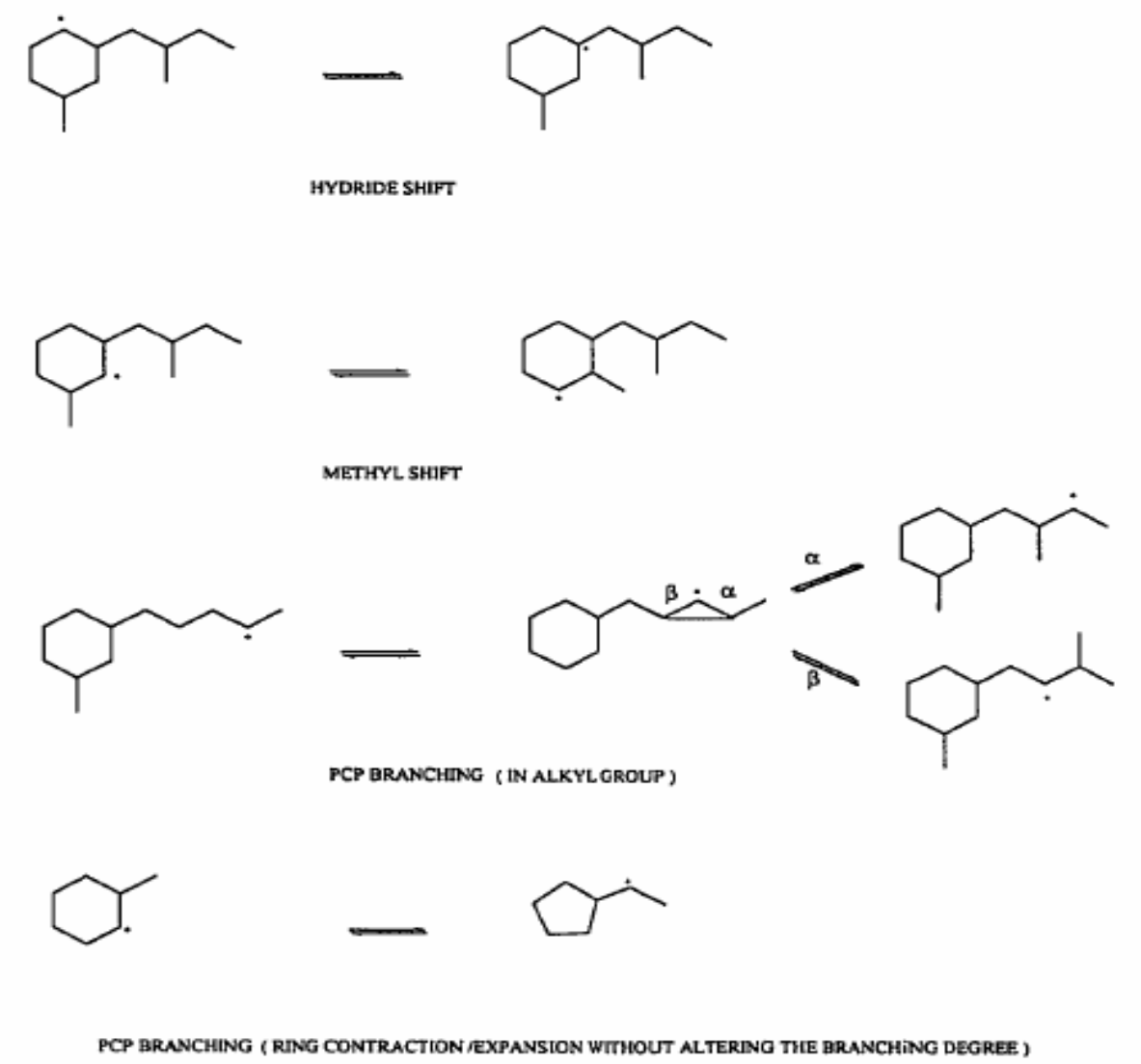

Fig. 2.4 Elementary Steps of Naphthene Isomerization (Martens et al., 2001)

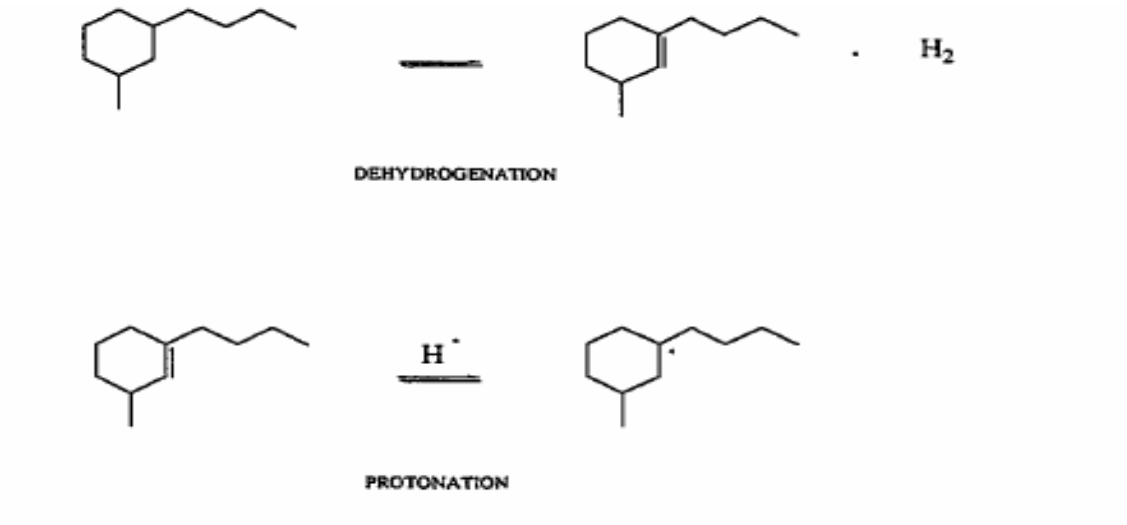

Fig. 2.5 Elementary Steps of Naphthene Dehydrogenation (Moustafa and Froment, 2003)

The three different types of PCP steps and their resulting effects on the naphthenes undergoing hydroisomerization are shown in Table 2.1.

Table 2.1. PCP Steps of the Hydroisomerization of Naphthenes

PCP STEP	**Ring Contraction or Expansion**	**Branching Effects**
(1).Acyclic PCP Branching	No ring contraction or expansion	Branching on alkyl side chain
(2). Intra-Ring Alkyl Shift	Ring contraction & expansion	No alteration in degree of branching
(3). Cyclic PCP Step	Ring contraction & expansion	Alters degree of branching on ring

Vynckier and Froment (1991) formulated that two types of β-scission are possible in the hydrocracking of naphthenes. Naphthenic carbenium ions undergo endocyclic β-scission and exocyclic β-scission. If β-scission occurs on alkyl side chain or if the alkyl side chain is severed it is known as exocyclic β-scission, and cleavage of a C-C bond within the ring is termed endocyclic β-scission. Exocyclic β-scission produces an olefinic and a cationic species of reduced carbon number. Endocyclic β-scission produces a single species containing a double

bond and a positively charged carbon atom. The cyclo-alkane carbenium ions formed from endocyclic β-scission may further undergo steps similar to those of cyclo-alkane carbenium ions shown in Fig. 2.6.

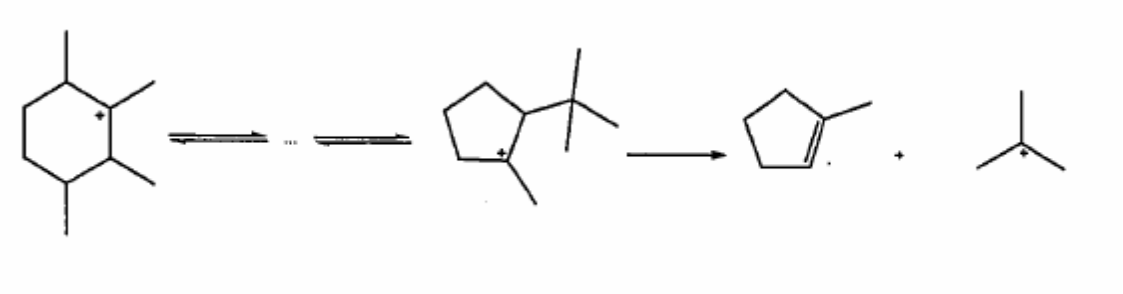

Fig. 2.6. Paring Reaction of Cyclo-Alkane Carbenium Ion (Martens et al., 2001)

The various cracking, deprotonation, branching, and hydrogenation steps involving naphthenes are shown in Fig 2.7. Cracking of naphthenes occurs by way of exocyclic and endocyclic β-scission. PCP branching of naphthenes results in both ring contraction and ring expansion altering the degree of branching.

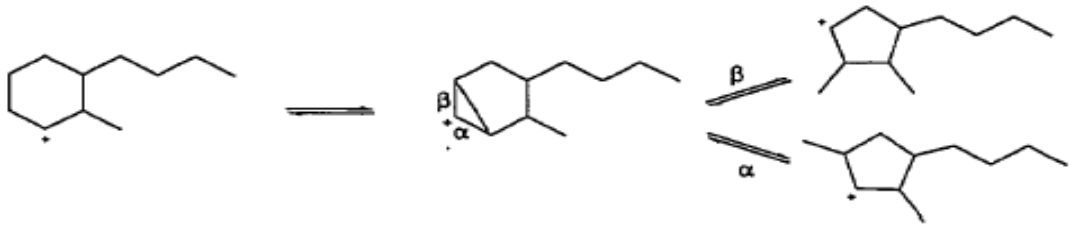

PCP BRANCHING (RING CONTRACTION / EXPANSION ALTERING THE BRANCHING DEGREE)

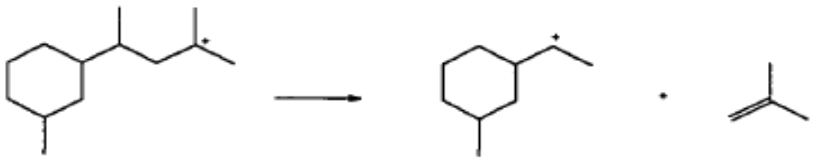

EXOCYCLIC β–SCISSION (IN ALKYL GROUP)

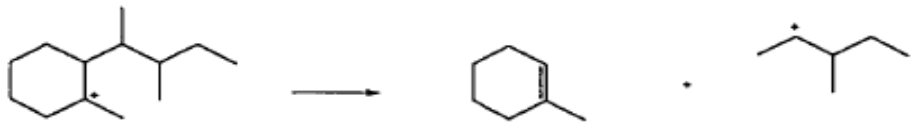

EXOCYCLIC β–SCISSION

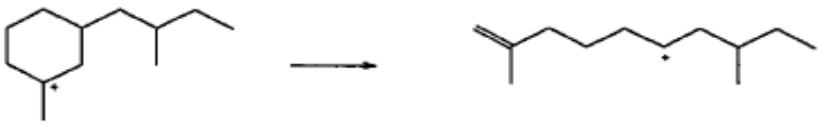

ENDOCYCLIC β -SCISSION

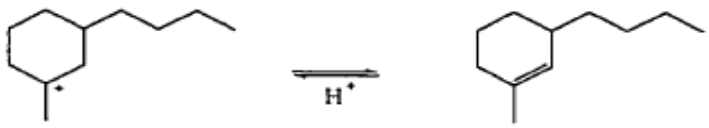

DEPROTONATION

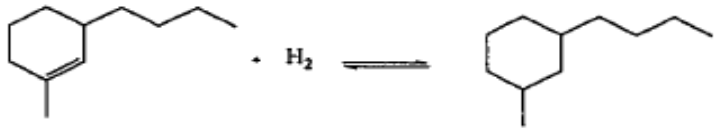

HYDROGENATION

Fig. 2.7. Elementary Steps of Naphthene Cracking (Vynckier and Froment, 1991)

The elementary steps involved in the hydrocracking of aromatics in HVGO are described in Figs. 2.8-2.11. Aromatics are rapidly hydrogenated and also dehydrogenated at metal sites on the catalyst.

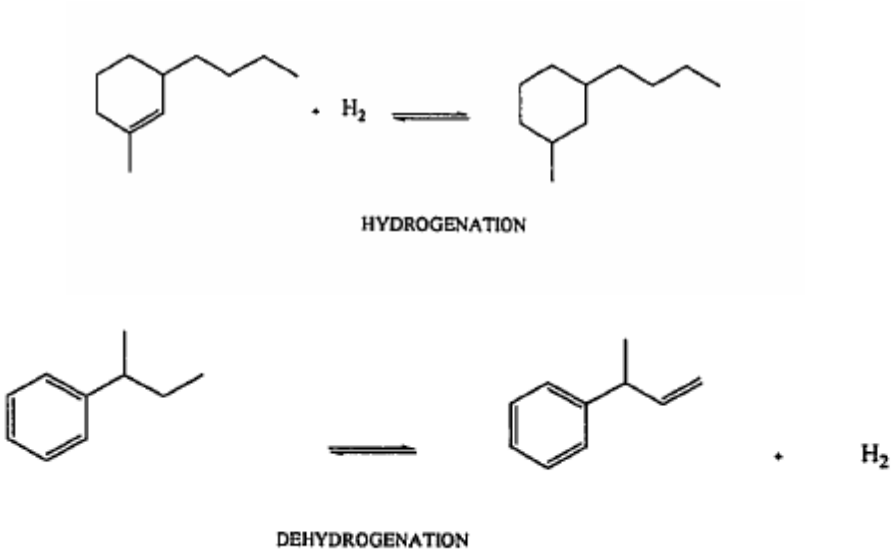

Fig. 2.8. Elementary Steps of Aromatic Hydrogenation (Vynckier and Froment, 1991)

The aromatic ring is not cleaved in hydrocracking; therefore the C-C bond cleaves only in side chains or naphtheno-aromatic components. Alkyl side chains undergo hydrogenation on catalyst metal sites to produce aromatic olefins, which further protonate on catalyst acid sites to form an aromatic carbenium ion. Aromatic carbenium ions with a positively charged alkyl group carbon atom isomerize through PCP branching, hydride shift and methyl shift, much the same way naphthenes isomerize.

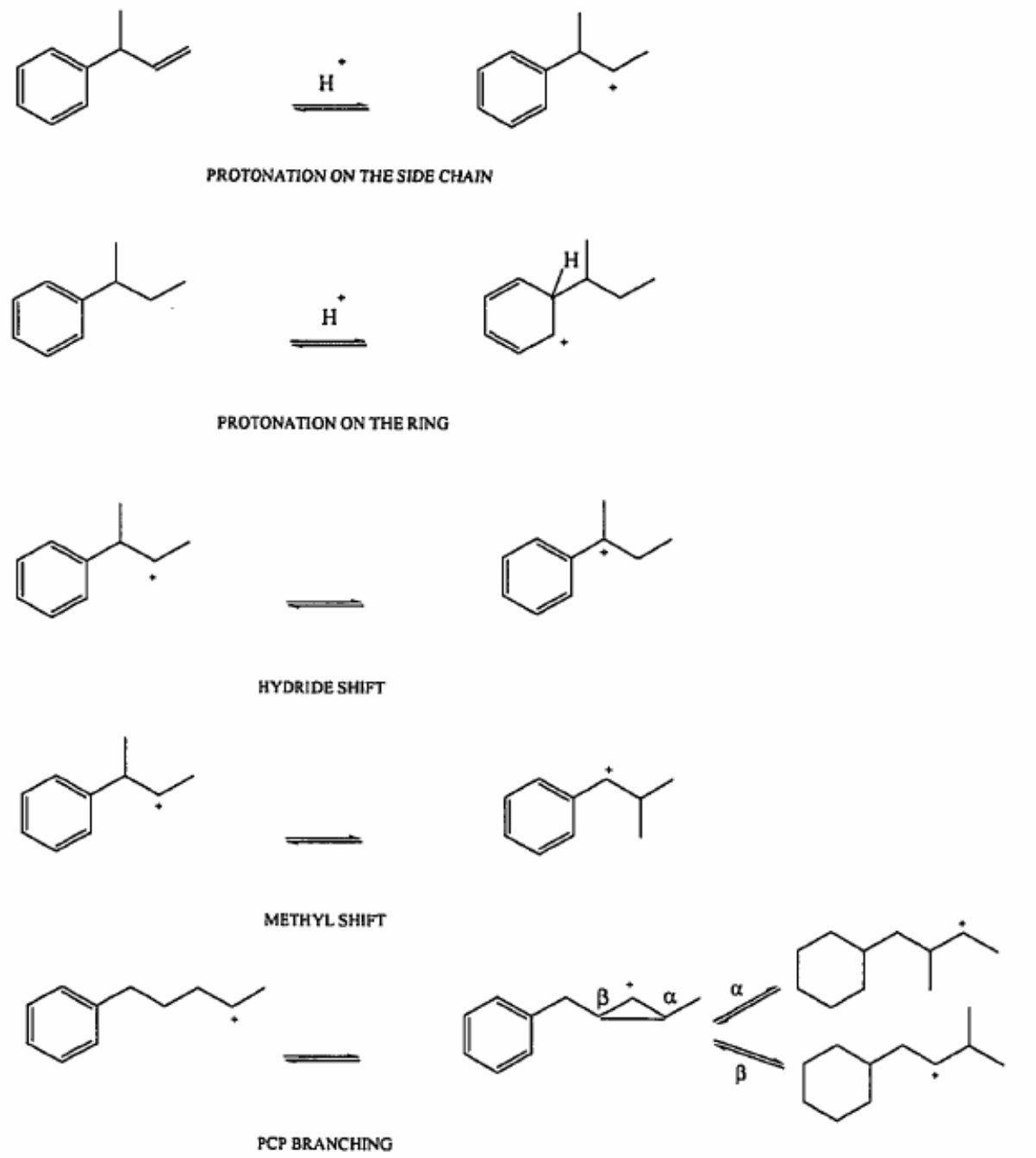

Fig. 2.9. Elementary Steps of Aromatic Isomerization (Moustafa and Froment, 2003)

Aromatics undergo alkylation and cyclization on metal loaded solid catalysts by way of Friedel-Crafts mechanism, and the cyclization reaction leads to the formation of naphtheno-aromatics. For cyclization to occur the reacting aromatic carbenium ion must have five or more carbon atoms in the alkyl chain with the positive charge suitably located.

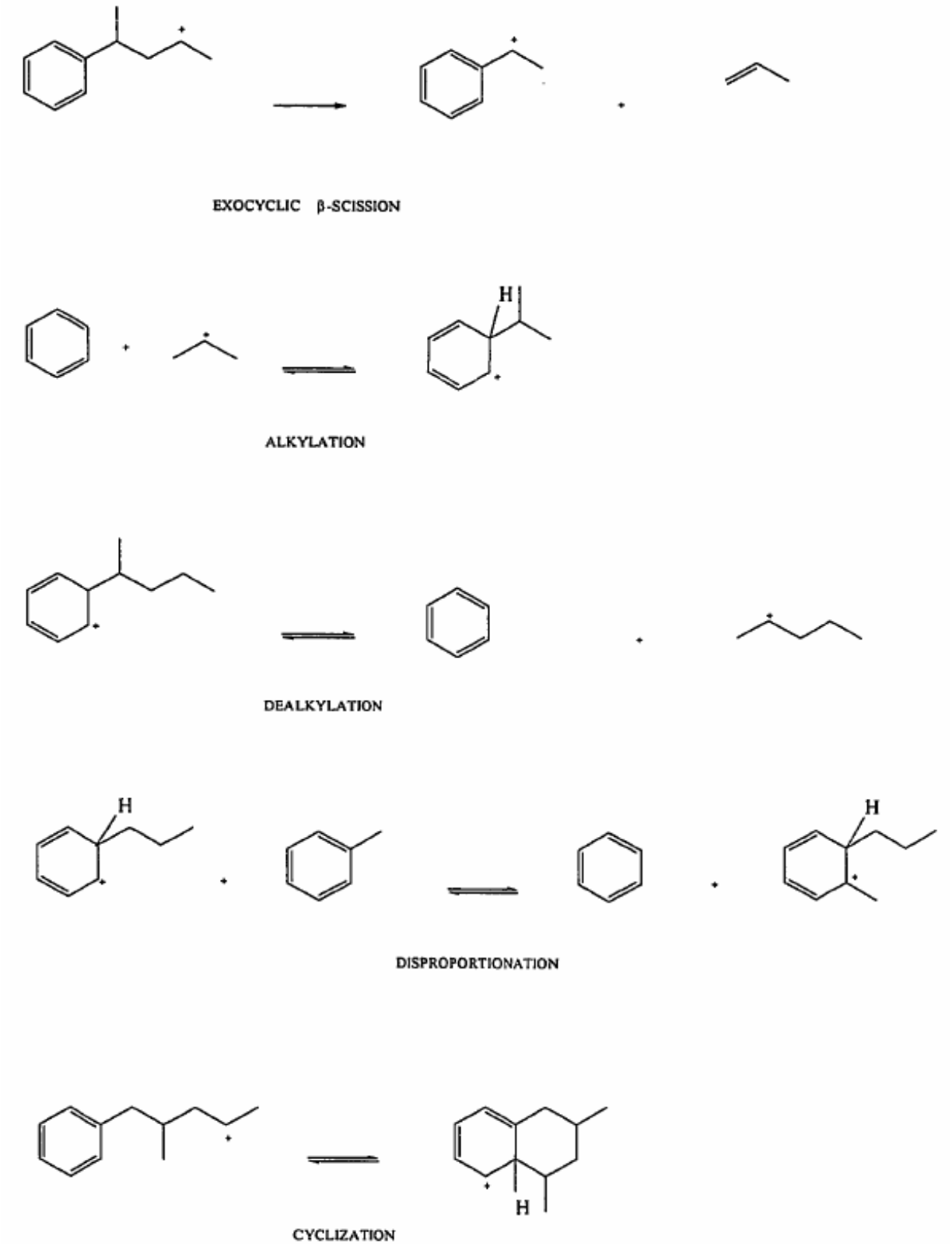

Fig. 2.10. Elementary Steps of Aromatic Cracking (Moustafa and Froment, 2003)

Aromatic carbenium ions with positively charged carbons on the ring deprotonate to produce aromatics, and aromatic carbenium ions with a positively charged alkyl side chain or a naphthenic component, deprotonate to yield the corresponding olefins which are rapidly hydrogenated on the metal site of the catalyst.

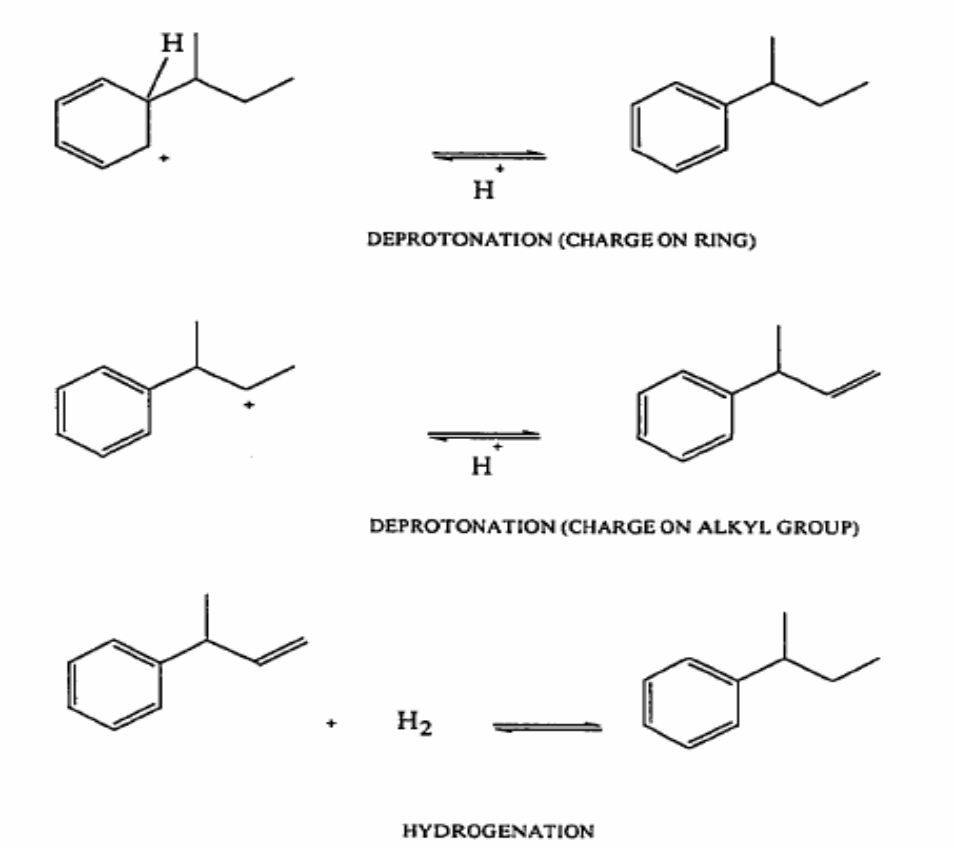

Fig. 2.11. Elementary Steps of Aromatic Deprotonation (Vynckier and Froment, 1991)

2.2 Single-Event Kinetics

The single-events kinetic theory developed by Vynckier and Froment (1991) formulates the rate coefficient for an elementary step into two parts.

$$k = n_e k' \tag{2.1}$$

where k is the rate coefficient for an elementary step, n_e is the ratio of global symmetry numbers of the reactant and the activated complex, and k' is the single-event rate coefficient. Eq. (2.1)

can be derived from transition state theory. From transition state theory the rate coefficient of an elementary step can be written as,

$$k = \frac{k_B T}{h} \exp(\frac{\Delta S^{\circ\mp}}{R}) \exp(\frac{-\Delta H^{\circ\mp}}{RT}) \tag{2.2}$$

According to statistical thermodynamics, the standard entropy of a species is determined by the summation of translation, vibrational, and rotational contributions. The rotational contribution is composed of two terms the intrinsic value $\hat{S}^{\circ}$ and a term due to symmetry σ, which depends on the geometry of the molecule.

$$S^{\circ}_{rot} = \hat{S}^{\circ}_{rot} - R\ln(\sigma) \tag{2.3}$$

When accounting for the effects of chirality, the rotational contribution S°_{rot} is given by:

$$S^{\circ}_{rot} = \hat{S}^{\circ}_{rot} - R\ln(\frac{\sigma}{2^n}) \tag{2.4}$$

where *n* is the number of chiral centers in a particular species. The expression in the parenthesis is called the global symmetry number and can be further expressed by Eq. (2.5).

$$\frac{\sigma}{2^n} = \sigma_{gl} \tag{2.5}$$

The difference in standard entropy between reactant and the activated complex due to symmetry changes is given by:

$$\Delta S^{\circ\mp}_{sym} = R\ln(\frac{\sigma^{r}_{gl}}{\sigma^{\mp}_{gl}}) \tag{2.6}$$

Substituting this contribution into Eq. (2.2) results in:

$$k = (\frac{\sigma_{gl}^{r}}{\sigma_{gl}^{\mp}})\frac{k_B T}{h}\exp(\frac{\Delta S^{\circ\mp}}{R})\exp(\frac{\Delta H^{\circ\mp}}{RT}) \tag{2.7}$$

The rate coefficient of an elementary step can now be written in terms of the number of single events n_e and the single event rate coefficient k' as it was in Eq (2.1).

$$k = n_e k' \tag{2.8}$$

The rate coefficient of the elementary step now truly characterizes the reaction step at a fundamental level since the effect of structure between the reactant and the activated complex has been factored out by introducing the number of single events that are associated with the step. The calculation of the global symmetry numbers of the reacting and produced carbenium ions and the activated complex is determined by means of quantum chemical packages such as GAMESS, MOPAC, and GAUSSIAN (Alwahabi and Froment, 2004).

A single-event frequency factor that does not depend on the structure of the reactant and the activated complex, and is unique for a particular elementary step can be defined as:

$$\tilde{A} = \frac{k_B T}{h}\exp(\frac{\Delta S^{\circ}}{R}) \tag{2.9}$$

To reduce the correlation between pre-exponential factors and activation energies re-parameterization has been applied (Park and Froment, 2001). The Arrhenius form of the single-event rate coefficient is given by:

$$k' = \tilde{A}\exp(\frac{E_a}{RT}) \tag{2.10}$$

Introducing the mean temperature, *Tm*, the single-event rate coefficient is:

$$k' = \exp\left[\left(\ln \widetilde{A}_i - \frac{E_{ai}}{RT_m}\right) - \frac{E_{ai}}{R}\left(\frac{1}{T} - \frac{1}{T_m}\right)\right] \tag{2.11}$$

The single-event rate coefficient can also be expressed by parameters devised by Park and Froment (2001), to take the place of the temperature independent portions of Eq. (2.11).

$$k' = \exp\left[\beta_i - \beta_k\left(\frac{1}{T} - \frac{1}{T_m}\right)\right] \tag{2.12}$$

2.3 Thermodynamic Constraints on Rate Parameters

Even though use of the single-event concept along with reparameterization described by Park and Froment (2001), resulted in significant reduction in the number of rate parameters needed to model the hydrocracking of a HVGO, a large number of equilibrium constants remain to be estimated. It is assumed that the rate coefficient for prototnation of olefins/cyclic olefins does not depend on the olefin, because the structure of the activated complex does not vary significantly from that of the reacting olefin/cyclic olefin. This is justified by the results of quantum chemical software (Moustafa and Froment, 2003). The equilibrium constant for isomerization of the olefin O_1 into O_2 proceeding over a secondary carbenium ion can be written as:

$$K_{isom}(O_1 \Leftrightarrow O_2) = \frac{k_{\mathrm{Pr}}(O_1; s)}{k_{Dep}(s; O_1)} \frac{k_{Dep}(s; O_2)}{k_{\mathrm{Pr}}(O_2; s)} \tag{2.13}$$

After incorporating the above mentioned constraint concerning the structural similarity of the reactant and activated complex of the protonated olefin Eq. (2.14) is obtained.

$$k_{Dep}(m; O_j) = k_{Dep}(m; O_r) K_{isom}(O_r \Leftrightarrow O_j) \tag{2.14}$$

The subscript *m* represents a secondary or a tertiary carbenium ion and O_r is a reference olefin with the double bond in a position such that the secondary and tertiary ions can be formed

from protonation (Moustafa and Froment, 2003). From the relationship expressed in Eq. (2.14) it can be determined that within a given carbon number, there are only two independent rate coefficients for deprotonation: $k_{Dep}(s;O_r)$ and $k_{Dep}(t;O_r)$. From an analysis of equilibria in a reaction sequence consisting of olefin protonation, carbenium ion isomerization and deprotonation, Baltanas et al. (1989) derived the following relationship for the ratio between single event isomerization steps.

$$\frac{k_{iosm}(t;s)}{k_{isom}(s;t)} = \frac{k_{\Pr}(s)}{k_{\Pr}(t)} \frac{k_{Dep}(t;O_r)}{k_{Dep}(s;O_r)} \tag{2.15}$$

The relationship expressed in Eq. (2.15) reduces the number of independent rate coefficients for all PCP branching, methyl shift, and hydride shift that undergo the above mentioned reaction sequence. Further more, the ratio of deprotonation coefficients in Eq. (2.15) have to be identical for all reference olefin, regardless of carbon number because the ratio of protonation and isomerization rate coefficients are independent of olefin. From an analysis of the structures of the reactant olefins and the corresponding activated complex involved in the protonation, deprotonation, and isomerization steps in hydocracking, it follows that for a given carbon number, there are only two independent single-event rate coefficients for deprotonation, and isomerization elementary steps.

2.4 Paraffin, Olefin, and Carbenium Ion Single-Event Rate Equations

According to Baltanas et al. (1989) in the hydrocracking reaction network, paraffins are generated by hydrogenation of olefins and are consumed by dehydrogenation.

$$P_i \leftrightarrow O_{ij} + H_2 \tag{2.16}$$

The olefin produced from paraffinic species *i* is denoted by an *O*, and the subscript *j* in the product olefin denotes that one paraffin can produce several olefins. A distinction must be made between the olefin isomers, because the position of the double-bond determines which carbenium ions can be formed from the olefin. Because different elementary steps are associated

with different double-bond isomers, it is not necessary to distinguish between geometric isomers (Baltanas et al., 1989). The net rate of formation of paraffins is then represented by:

$$R_{P_i} = \sum_j [k_H(ji) C_{O_{ij}} p_{H_2} - k_{DH}(ij) C_{P_i}] \tag{2.17}$$

Olefins which are formed on the metal site of the catalyst are then protonated on the acid sites. Two carbenium ions result.

$$\begin{aligned} O_{ij} + H^+ &\leftrightarrow R^+_{ij,m_1} \\ &\leftrightarrow R^+_{ij,m_2} \end{aligned} \tag{2.18}$$

The subscripts m_1 and m_2 refer to the type of carbenium ion, and only the protonation reactions producing the more stable secondary and tertiary carbenium ion are considered. Protonation of light olefins (C_8 and below), are also excluded from the reaction network (Baltanas et al., 1989).

For the hydrocracking reaction network it is important to include the formation of olefin O_{ij} as a result of carbenium ion cracking.

$$R^+_v \rightarrow O_{ij} + R^+_w \tag{2.19}$$

From Eq (2.19) the general expression for the net rate of formation of an olefin becomes:

$$\begin{aligned} R_{O_{ij}} = {} & k_{DH}(ij) C_{P_i} - k_H(ji) C_{O_{ij}} p_{H_2} + k_{De}(m_1; O_{ij}) C_{R^+_{ij,m_1}} + k_{De}(m_2; O_{ij}) C_{R^+_{ij,m_2}} \\ & - [k_{\mathrm{Pr}}(m_1) + k_{\mathrm{Pr}}(m_2)] C_{O_{ij}} C_{H^+} + k_{Cr}(v; w; O_{ij}) C_{R^+_v} \end{aligned} \tag{2.20}$$

By applying the pseudo-steady-state approximation to the olefin intermediates, the net rates of formation of the olefins is zero (Baltanas et al., 1989).

$$R_{O_{ij}} = 0 \tag{2.21}$$

If the rate determining step is located on the acid sites of the catalyst and Eqs. (2.17), (2.20), and (2.21) are combined, the net rate of formation of paraffins becomes:

$$R_{P_i} = \sum_j \{k_{De}(m_1; O_{ij}) C_{R^+_{ij,m_1}} + k_{De}(m_2; O_{ij}) C_{R^+_{ij,m_2}}$$

$$- [k_{\mathrm{Pr}}(m_1) + k_{\mathrm{Pr}}(m_2)] C_{O_{ij}} C_{H^+} + k_{Cr}(v; w; O_{ij}) C_{R^+_v}\} \quad (2.22)$$

Each rate coefficient in Eq. (2.22) and each rate coefficient in the following rate equations are derived as the product of the single event rate constant k' and number of single events n_e. The general rate equation describing the formation of carbenium ions is as follows:

$$R_{R^+_m} = \{\sum_O k_{\mathrm{Pr}}(m) C_O C_{H^+} + \sum_q k_{HS}(q; m) C_{R^+_q}$$

$$+ \sum_r k_{MS}(r; m) C_{R^+_r} + \sum_u k_{PCP}(u; m) C_{R^+_u}$$

$$+ \sum_v k_{Cr}(v; m, O') C_{R^+_v}\} - \{\sum_O k_{De}(m; O) + \sum_q k_{HS}(m; q)$$

$$+ \sum_r k_{MS}(m; r) \sum_u k_{PCP}(m; u) + \sum_z k_{Cr}(m; z, O')\} C_{R^+_m} \quad (2.23)$$

The pseudo-steady-state approximation was applied to calculate the concentration of inaccessible carbenium ions.

$$R_{R^+_m} = 0 \quad (2.24)$$

Eq. (2.25) introduces the total concentration of active sites on the catalyst (C_t), which is equal to the number of occupied plus unoccupied sites by carbenium ions.

$$C_t = C_{H^+} + \sum_m C_{R^+_m} \quad (2.25)$$

Plugging the concentrations relative to vacant acid sites: $C^*_{H^+} = \frac{C_{H^+}}{C_t}$; $C^*_{R_m^+} = C_{R_m^+} / C_t$ into Eq. (2.25), leads to Eq. (2.26), which relayes the concentration of vacant acid sites to that of each species.

$$C^*_{H^+} = 1 - \sum_m C^*_{R_m^+} \tag{2.26}$$

A modified set of rate coefficients that incorporate the total number of active sites can now be plugged back into Eq (2.23), which is the rate expression for carbenium ion formation and consumption.

Employing the appropriate pseudo-steady-state assumptions mentioned above, and rearranging into a set of linear equations allows for the calculation of the relative concentrations of carbenium ions in terms of olefin concentrations. Relative concentrations of carbenium ions and free sites are then substituted into the rate expression of the formation and consumption of paraffins (Eq. (2.22)). The result is an expression expressing the net rate of formation of paraffins in terms of the sorbed olefin concentrations (Baltanas et al., 1989)

$$C_{O_{ij}} = \frac{C_{P_i} K_{D,H,ij}}{p_{H_2}} \tag{2.27}$$

Through thermodynamic state functions the equilibrium constants for dehydrogenation $K_{DH,ij}$ can be calculated. Sorption into the zeolite cage is assumed to be in quasi-equilibrium, and it is described by using a Langmuir isotherm.

$$C_{O_{ij}} = \frac{C_{s,sat} K_{L,i} K_{DH,ij} p_i}{1 + \sum_m K_{L,m} p_m} \tag{2.28}$$

$C_{s,sat}$ is the unknown saturation concentration of sorbed hydrocarbons, and it is lumped into the rate constant which multiplies the olefin concentration.

Since light hydrocarbon species are further from saturation then heavy hydrocarbons, sorption of all compounds lighter than C_6 may be disregarded above 459 K. By combining Eq. (2.26) and (2.27) the olefin concentration can be expressed in terms of the partial pressure of hydrocarbons and hydrogen, which are observable quantities (Baltanas et al., 1989).

$$C_{O_{ij}} = \frac{C_{s,sat} K_{L,i} K_{DH,ij} p_i}{p_{H_2} (1 + \sum_m K_{L,m} p_m)} \tag{2.29}$$

2.5 Multiphase Operations

The mass transfer of hydrogen from the gas phase through the liquid to the metal sites on the catalyst is expressed in terms of the two film theory (Froment and Bischoff, 1990). Hydrogen in the gas phase experiences mass transfer resistance approaching the gas/liquid interface of the film. At the interface there is no resistance to mass transfer so that Henry's law is satisfied.

$$p_{Ai} = HC_{Ai} \tag{2.30}$$

These mass transfer coefficients are functions of the properties of the involved species and of the flow conditions. Correlations can be found in the literature (Treybal, 1980). Hydrogen in the liquid phase then adsorbs and reacts with adsorbed species on the catalyst metal sites. If the catalyst is sufficiently loaded with metal the hydrogenation and dehydrogenation steps in the hydrocracking reaction network are in quasi-equilibrium and the rate determining step lies at the acid sites of the catalyst.

Hydrogen is not the only component that is transferred from the gas phase through the liquid. Lighter hydrocarbon products (C_{10} and below) can also be transferred from the liquid phase to the gas phase after desorbing from the zeolite cage. After sorption, isomerization, β-scission, and hydrogenation steps, heavy paraffins can form lighter paraffins that desorb from the zeolite cage, transfer through the liquid phase and into the gas phase. The lighter components in the gas phase are in equilibrium with those in the liquid phase and Henry's law is satisfied at the gas/liquid interface. The heterogeneous mass and energy continuity equations for the hydrocracking of HVGO are given in Eqs. (2.31) through (2.35).

continuity equation for hydrogen in the gas phase:

$$\frac{1}{\Omega}\frac{dF_i}{dz} = -(K_g a_v)[(p_g)_i - H_i(C_l)_i] \tag{2.31}$$

continuity equation for light hydrocarbon components in the gas phase:

$$\frac{1}{\Omega}\frac{dF_i}{dz} = (K_g a_v)[(p_g)_i - H_i(C_l)_i] \tag{2.32}$$

continuity equation for components in the liquid phase:

$$\frac{1}{\Omega}\frac{dF_i}{dz} = (K_l a_v)[(C_l)_i - \frac{(p_g)_i}{H_i})] + \rho_B \sum_{j=1}^{N_R} s_i r_j \tag{2.33}$$

where F_i is the molar flow rate of component i, a_v is the interfacial surface area per m^3 reactor, s_i is the stoichiometric coefficient for component i in reaction j, K_g and K_l are the overall mass transfer coefficients between the bulk phase of the gas and the liquid.

gas phase energy equation:

$$[\frac{\dot{m}_g C_{pg}}{\Omega}]\frac{dT}{dz} = h_g a_v (T_g - T_l) \tag{2.34}$$

liquid phase energy equation:

$$[\frac{\dot{m}_l C_{pl}}{\Omega}]\frac{dT}{dz} = \rho_B \sum_{j=1}^{N_R} r_j(-\Delta H_j) + h_l a_v (T_l - T_g) \tag{2.35}$$

In Eqs. (2.34) and (2.35), h_l and h_g are overall heat transfer coefficients between the bulk phase of gas and liquid. The boundary conditions for the set of continuity equations are shown below:

$$z = 0 \qquad \begin{aligned} (p_g)_i &= (p_g^\circ)_i \\ (C_l)_i &= (C_l^\circ)_i \\ T_l &= T_l^\circ \\ T_g &= T_g^\circ \end{aligned} \tag{2.36}$$

By use of curve 1 in Fig. 3.2.1-1 in Froment and Bischoff (1990), experimental results for values of j_D factor can be obtained, which is used to obtain the mass transfer coefficient between the fluid and the bed of particles.

$$j_D = \frac{k_g M_m}{G} Sc^{2/3} \tag{2.37}$$

By use of curve 4 in Fig 3.2.2-1 in Froment and Bischoff (1990), experimental results for values of the j_H factor can be obtained, which is used to calculate the heat transfer coefficient between the fluid and the bed of particles.

$$j_H = \frac{h_f}{C_P G} \mathrm{Pr}^{2/3} \tag{2.38}$$

CHAPTER III
SINGLE-EVENT MODEL RESULTS

3.1 Simulation of Isothermal Hydrocracking of HVGO

The following section includes the results of the isothermal hydrocracking of HVGO. The hydrocracking of HVGO is performed in three-phase (gas-solid-liquid) fixed bed trickle flow reactors, with hydrogen transferring from the gas through the liquid phase to metal sites on a solid catalyst. The three phases correspond to a fixed bed of porous catalyst particles, a vapor phase containing high partial pressures of hydrogen and low partial pressures of vaporized light hydrocarbons, and a liquid phase that consists of hydrogenated vacuum gas oil components. The feed composition and the reactor operating conditions were obtained from a pilot scale reactor. A single-event kinetic model, formulated by Froment and coworkers, was used to simulate the hydrocracking and to predict the product distribution along the length of the reactor. The evolution of products predicted by the model is compared to the isothermal data provided from a pilot reactor.

The following assumptions have been made in the development of the reactor model:

(1). A plug flow pattern for the gas and liquid phase exists in the trickle flow reactor.

(2). Heat loss is negligible.

(3). Operation is at steady-state.

(4). Pressure drop in reactor is negligible.

(5). Deactivation of catalyst is negligible.

The reactor and operating conditions are described in Table 3.1. The reactor cross sectional area is denoted by Ω, the reactor length is designated by z, and the reactor diameter is designated by D.

Table 3.1. Isothermal Operating Conditions

Reactor Type:	tubular, 3 phase, isothermal, trickle flow
Reactor Dimensions:	$\mathbf{\Omega} = 5.1*10^{-4}$ m^2; $\mathbf{z}$ = 2.63 m; $\mathbf{D}$ = 0.0254m
Inlet Pressure:	$\mathbf{P_i}$ =160 bar
Reactor Temperature:	$\mathbf{T_r}$ = 350 C
Liquid Molar Feed Rate:	$\mathbf{F} = 1.7*10^{-3}$ kmol/hr
Hydrogen/ Feed Molar Ratio:	$\boldsymbol{\gamma}$ = 30 kmol/kmol
Bulk Density of Catalyst:	$\boldsymbol{\rho_B}$ = 0.4155g/cc cat

The composition of the liquid feed was formulated from an industrial HVGO feed stock, and was arranged into 241 components and lumps in the gas phase and 241components and lumps in the liquid phase up to carbon number 33. The feed stock composition used in the model and in the pilot reactor is shown in Table 3.2. The present research considers up to four rings in cyclic hydrocarbon structures, and the various types of components and lumps that can be formed as products in hydrocracking are: iso-paraffins, normal paraffins, mono, di, tri, terta-naphthenes, mono, di, tri, tetra-aromatics, naphtheno-mono, naphtheno-di, and naphtheno-tri aromatics.

In a hydrocracking reaction network generation of a C_{33} HVGO feed, the number of elementary steps is anywhere from 2,886,158 steps to 3 million steps, with 836,693 protonation steps, 837,015 deprotonation steps, 761,712 hydride shifts, 89,960 methyl shifts, 275,176 protonated cyclo-propane branching steps, and 85,602 β-scission steps. There are 396,354 carbenium ions and 448,395 olefins involved in the reaction network of the hydrocracking of a C_{33} feed. Within this work the various commercial petroleum fractions are defined as follows:

LPG	C_3-C_4
LNAP	C_5-C_7
HNAP	C_{8}-$_{12}$
KERO	C_{13}-C_{15}
MDS	C_{16}-C_{24}
Residue	$> C_{24}$

LPG is light petroleum gas, LNAP is light naphtha, HNAP is heavy naphtha, KERO is kerosene, and MDS is middle distillates.

Table 3.2. Liquid HVGO Composition

no. of C	nPar	iPar	MNA	DNA	TNA	QNA	MAR	DAR	TAR	QAR	NMA	DNMA	NDA	sum
7	0.030		0.107											0.137
8	0.053	0.023	0.335											0.411
9	0.061	0.061	0.510											0.632
10	0.129	0.099	0.564	0.305										1.097
11	0.366	0.206	0.640	1.120				0.003			0.002			2.336
12	0.670	0.388	0.670	1.279			0.012	0.002			0.014			3.037
13	0.647	0.586	0.640	1.081			0.005	0.014			0.029			3.002
14	0.282	0.366	0.411	0.807	0.419		0.046	0.012			0.145	0.048	0.023	2.559
15	0.213	0.206	0.312	0.670	0.746		0.051	0.019	0.003		0.150	0.098	0.050	2.519
16	0.221	0.160	0.259	0.503	0.663		0.054	0.026	0.006		0.155	0.088	0.064	2.198
17	0.221	0.168	0.244	0.411	0.678		0.066	0.038	0.015		0.195	0.136	0.093	2.264
18	0.251	0.175	0.228	0.320	0.625	0.015	0.076	0.060	0.026	0.006	0.226	0.176	0.138	2.323
19	0.274	0.190	0.228	0.274	0.526	0.030	1.607	1.240	0.668	0.603	3.144	1.337	1.700	11.822
20	0.289	0.198	0.244	0.251	0.426	0.038	0.107	0.114	0.058	0.035	0.279	0.224	0.205	2.470
21	0.396	0.221	0.289	0.259	0.373	0.061	0.000	0.000	0.000	0.000	0.000	0.000	0.000	1.599
22	0.503	0.282	0.335	0.274	0.343	0.053	1.356	1.050	0.700	0.360	2.501	2.227	1.640	11.624
23	0.739	0.388	0.449	0.327	0.343	0.099								2.346
24	1.021	0.526	0.571	0.419	0.289	0.122								2.947
25	1.318	0.701	0.754	0.495	0.434	0.168								3.869
26	1.622	0.830	0.876	0.533	0.434	0.190								4.486
27	1.668	0.937	0.944	0.594	0.495	0.320								4.958
28	1.775	1.066	0.960	0.617	0.480	0.289								5.186
29	1.554	0.914	0.883	0.571	0.472	0.411								4.806
30	1.348	0.815	0.739	0.465	0.366	0.366								4.097
31	1.188	0.708	0.670	0.434	0.297	0.297								3.595
32	2.064	1.668	1.516	1.036	0.746	0.434								7.464
33	1.478	1.318	1.249	0.861	0.678	0.267								5.849
sum	20.38	13.20	15.63	13.90	9.83	3.16	3.38	2.58	1.48	1.00	6.84	4.33	3.91	100

Fifty single-event parameters were used in the model to simulate the isothermal hydrocracking of the HVGO, and they are described in Tables. 3.2-3.6. Kij is the equilibrium constant [dimensionless], and k_{ij} is the single-event parameter [kmol/kgcat*hr] for each respective elementary step in Tables 3.2-3.6. The single-events associated with isomerization and alkylation of molecules in the hydrocracking reaction network is described in Table 3.3.

Table 3.3 Single-Event Parameters for Isomerization & Alkylation

Single Event	Elementary Step	k_{ij} [kmol/kgcat*hr]
MS	sec-sec	equilibrium
MS	sec-tert	equilibrium
MS	tert-sec	equilibrium
MS	tert-tert	equilibrium
HS	sec-sec	equilibrium
HS	sec-tert	equilibrium
HS	tert-sec	equilibrium
HS	tert-tert	equilibrium
PCP	sec-sec	2.0
PCP	sec-tert	70.0
PCP	tert-sec	70.0
PCP	tert-tert	1750.0
(de)alkylation	sec	equilibrium
(de)alkylation	tert	equilibrium

The single-events associated with cracking of carbenium ions in the hydrocracking reaction network are described in Table 3.4. According to the rules that govern carbenium ion chemistry, the beta position with respect to the positive charge must be a tertiary or quaternary carbon atom for all carbon-carbon bond-breaking reactions. Furthermore, primary carbenium ions are discarded from the network entirely due to their lack of stability or high ionization energy. After applying the rules of carbenium ion chemistry and generating the reaction network, it was determined that particular single-event rate parameters associated with cracking of carbenium ions were insignificant in magnitude relative to other cracking steps, as shown in Table. 3.4.

Table 3.4 Single-Event Parameters for Cracking

Single Event	Elementary Step	k_{ij} [kmol/kgcat*hr]
β-scission	sec-sec, into n.o	~0
β-scission	sec-sec, into i.o	5000.0
β-scission	sec-tert, into n.o	~0
β-scission	sec-tert, into i.o	~0
β-scission	tert-sec, into n.o	~0
β-scission	tert-sec, into i.o	5000.0
β-scission	tert-tert, into n.o	~0
β-scission	tert-tert, into i.o	6.75×10^7
β-scission	endo-cyclic	3500.0

As discussed in section 2.4, within this research all hydrogenation and dehydrogenation are assumed to be in quasi-equilibrium and the equilibrium constants for hydrogenation and dehydrogenation of all possible hydrogenated species are calculated using available data and group contribution method.

Table 3.5 Single-Event Parameters for (De)Hydrogenation

Single Event	**Species Hydrogenated**	**K_{ij} [bar^{-1}]**
(de)hydrogenation	mar	equilibrium (10)
(de)hydrogenation	dar/tar/qar/nta	equilibrium (0.033)
(de)hydrogenation	nma	equilibrium (0.033)
(de)hydrogenation	nda	equilibrium (0.033)
(de)hydrogenation	dnma/dnda/tnma	equilibrium (0.033)

Section 2.5 showed that sorption into the zeolite cage can be described by using a Langmuir isotherm. Table 3.6 lists the single-event parameters associated with the sorption of all possible lumps recognized in the single-event model.

Table 3.6 Single-Event Parameters for Sorption

Single Event	**Species sorbed**	**k_{ij} [kmol/kgcat*hr]**
sorption	npa	0.025
sorption	ipa	0.02
sorption	mna	0.003
sorption	dna	0.003
sorption	tna	0.003
sorption	qna	0.003
sorption	mar	0.0035
sorption	dar	0.0035
sorption	tar	0.0035
sorption	qar	0.0035
sorption	nma	0.0035
sorption	nda	0.0035
sorption	nta	0.0035
sorption	dnma	0.0035
sorption	dnda	0.0035

Fig. 3.1 shows the evolution of the various commercial petroleum fractions along the length of the isothermal reactor, and when summed they result in 100 % yield of products. A 36.1% conversion occurs in the residue fraction which boils above 370^{o} C, and significant amounts of LPG and LNAP are formed along the reactor as heavier feed components are converted. Table 3.7 shows the percent yield of each crude oil fraction in the feed and at the exit of the reactor.

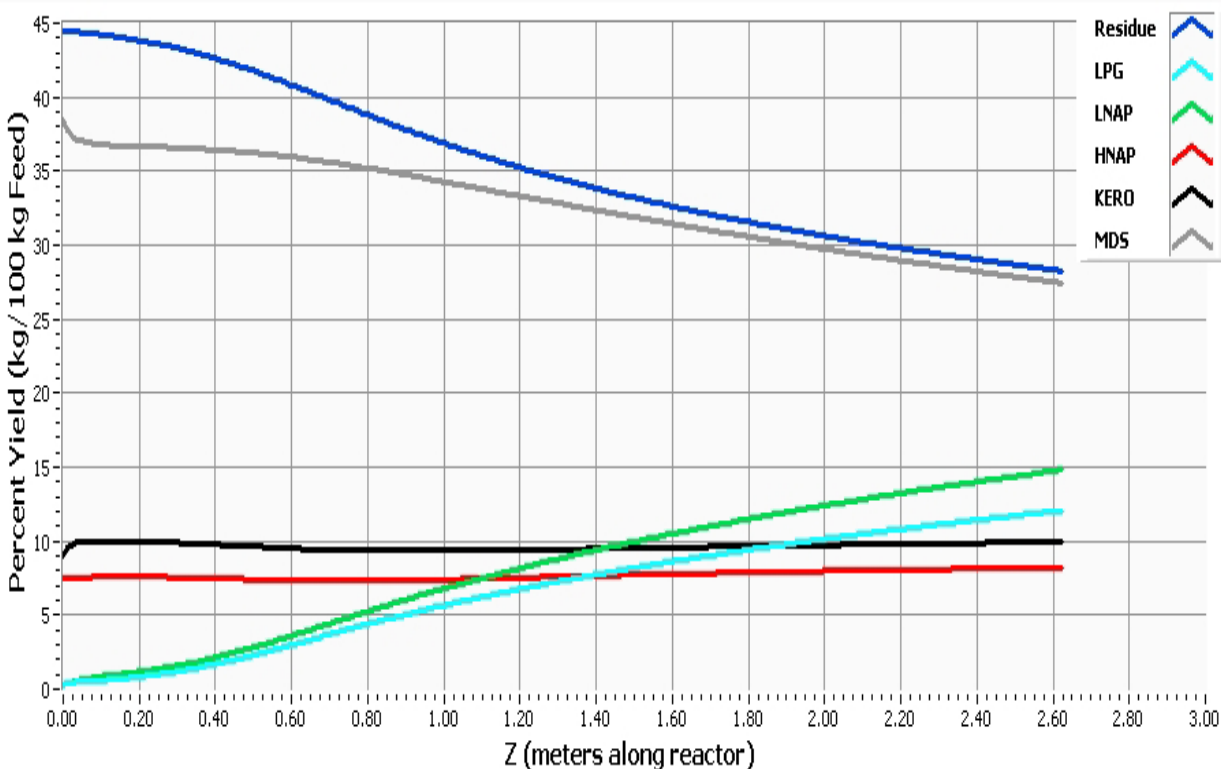

Fig. 3.1. Predicted Isothermal Evolution of Commercial Fractions

Table 3.7 Commercial Fraction in Feed and Product

Model Predictions	**Yield [kg/100 kg feed]**	**Yield [kg/100 kg feed]**
Fraction	Feed	Product
LPG (C_3-C_4)	0.5%	11.9%
LNAP (C_5-C_7)	0.8%	14.8%
HNAP(C_8-C_{12})	7.8%	8.1%
KERO(C_{13}-C_{15})	10.2%	9.8%
MDS (C_{16}-C_{24})	36.4%	27.1%
Residue (> C_{24})	44.3%	28.3%

Fig. 3.2 shows the evolution of mono, di, tri, and tetra-naphthenes along the length of the 2.63 meter reactor. Mono-naphthenes are formed as mono-aromatics are rapidly hydrogenated though the first half meter of the reactor. Di, tri, and tetra-aromatics are not as heavily hydrogenated as shown in Fig 3.3; therefore di, tri, tetra- naphthenes are not significantly produced throughout the reactor.

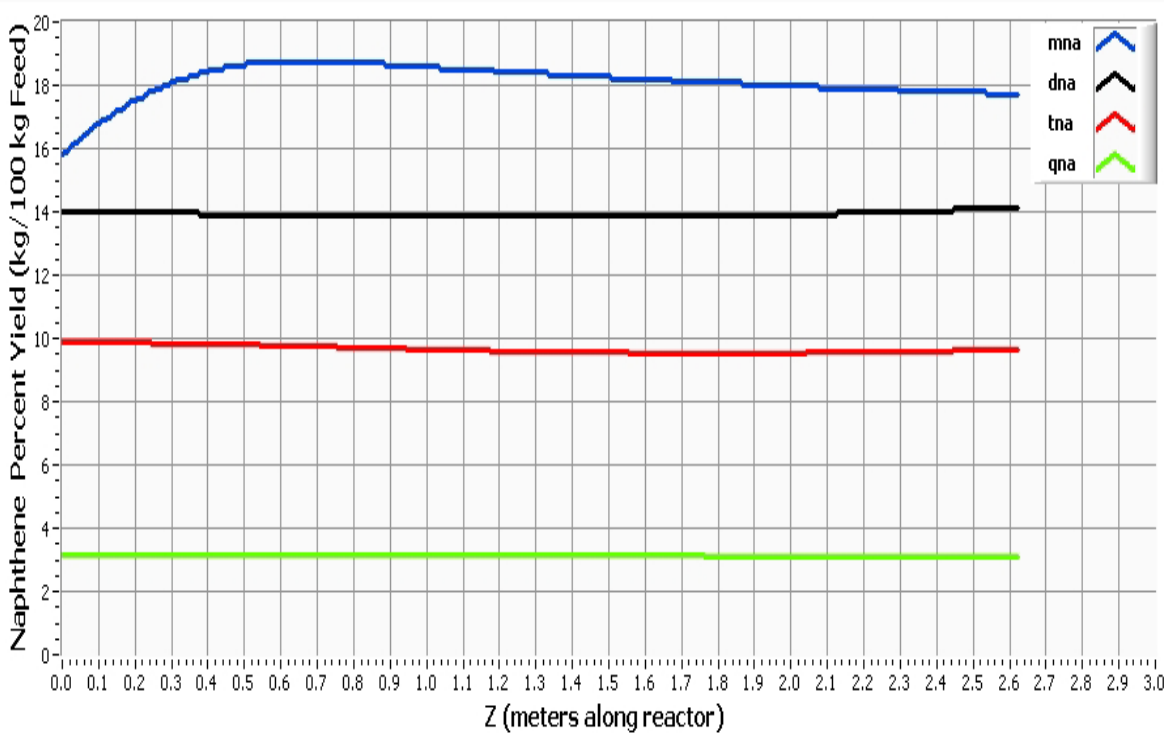

Fig. 3.2. Predicted Isothermal Evolution of Naphthenes

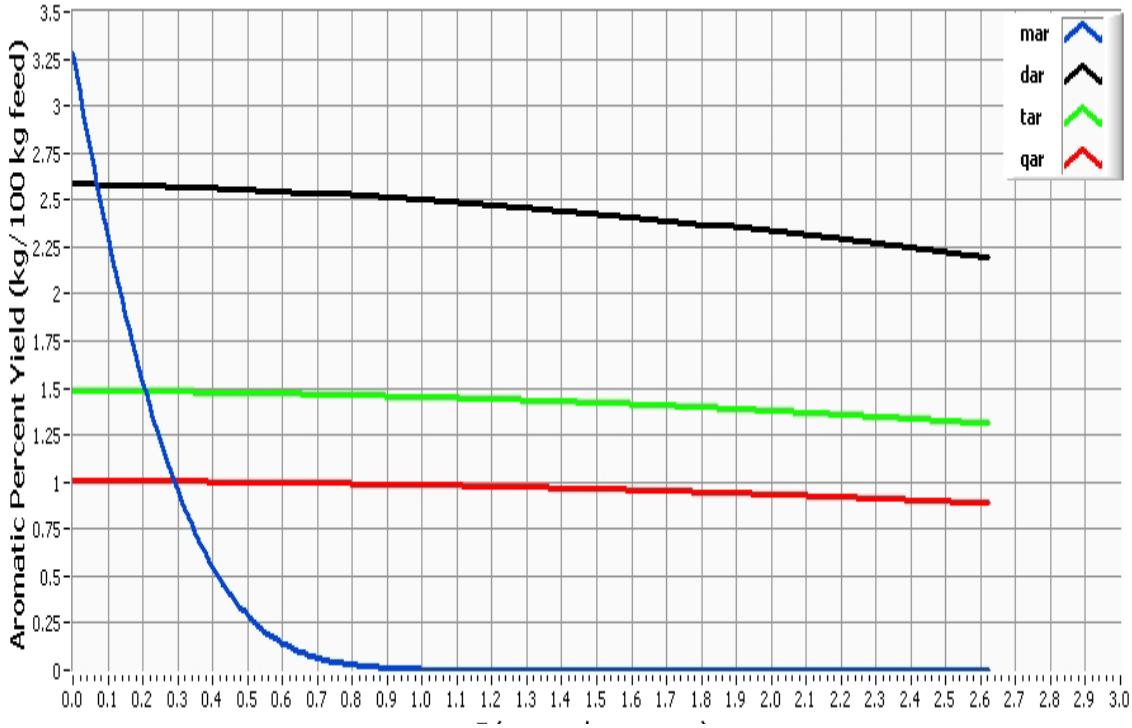

Fig. 3.3. Predicted Isothermal Evolution of Aromatics

Some production of di-naphthenes and tri-naphthenes is exhibited during reaction, which can be attributed to the hydrogenation of naphtheno mono-aromatic, naphtheno di-aromatics, and di-naphtheno mono-aromatics, which is shown in Fig. 3.4. A small amount of di-naphtheno di-aromatics and naphtheno tri-aromatics are formed from the partial hydrogenation of tetra-aromatics and cyclization of aromatic side chains.

The evolution of paraffins is shown in Fig. 3.5. A significant amount of iso-paraffins is produced along the reactor. Iso-paraffins are formed from cracking naphthenes with branched side-chains. The consumption of n-paraffins through PCP-branching also adds to the production of iso-paraffins.

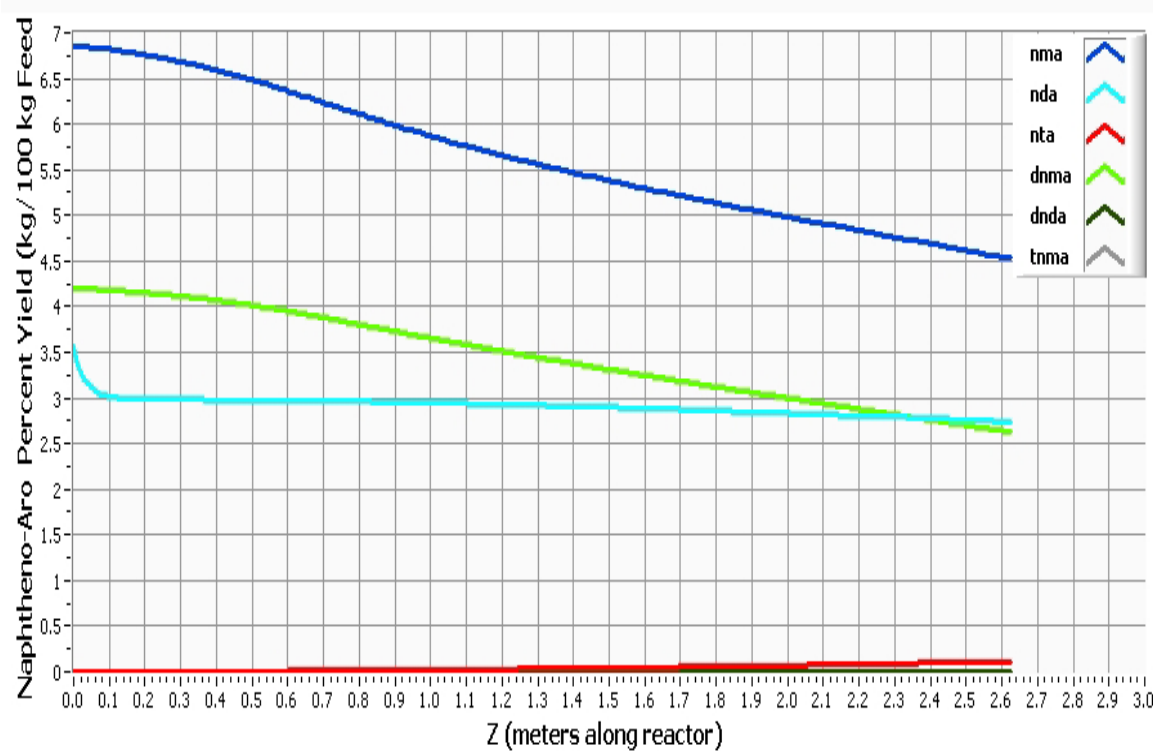

Fig 3.4 Predicted Isothermal Evolution of Naphtheno-Aromatics

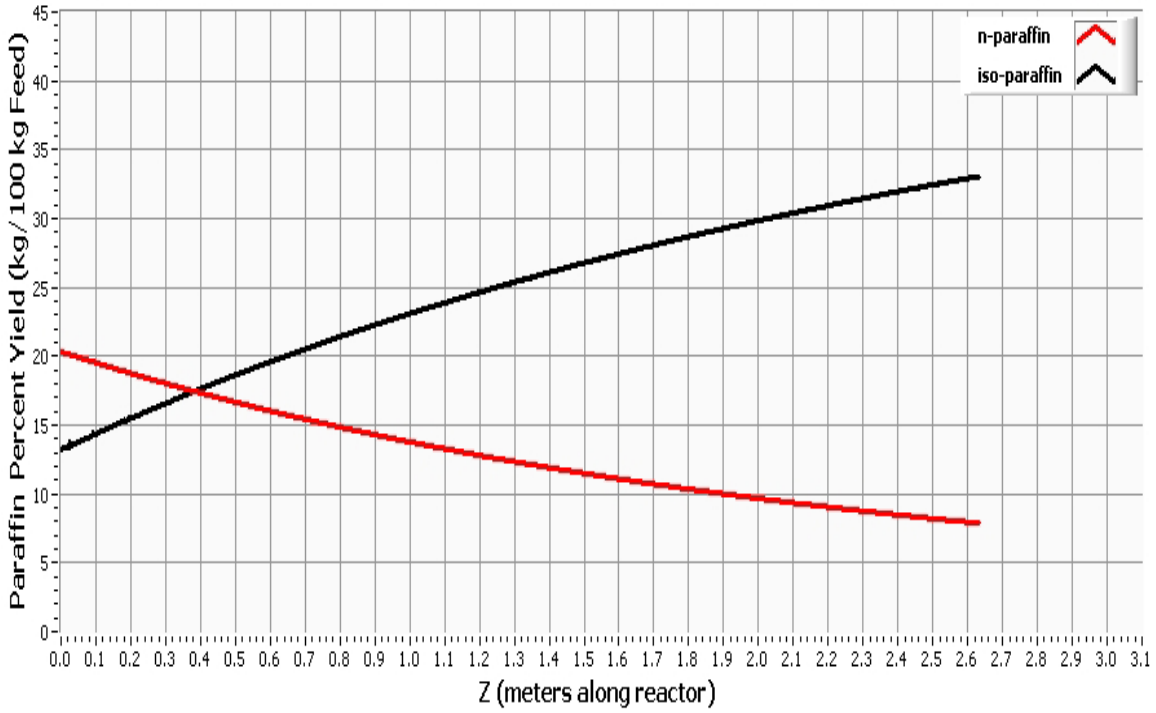

Fig 3.5 Predicted Isothermal Evolution of Paraffins

It is important to track the consumption of hydrogen in the liquid and gas phase since the reactions in the network progress by way of hydrogenation and dehydrogenation. Fig. 3.6 represents the hydrogen flux across the reactor, and shows that hydrogen in the liquid phase is consumed through the first 1.7 m of the reactor during the hydrogenation of aromatics. After the hydrogenation of aromatic and naphtheno aromatic species, the hydrogen in the liquid phase increases due to high solubility of gaseous hydrogen in liquid HVGO at 350^{o} C. The effects temperature on the solubility of hydrogen in HVGO will be further discussed in section 3.2.

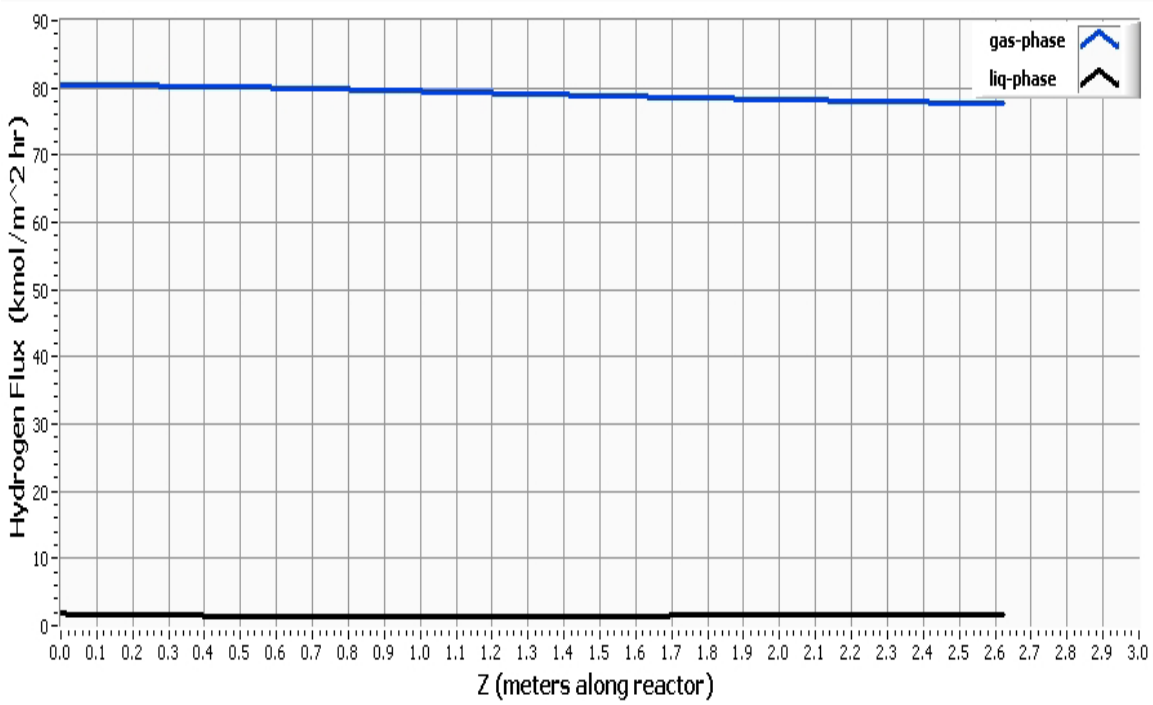

Fig 3.6 Predicted Isothermal Hydrogen Flux

The model and reactor simulation also has the capability of tracking the evolution of components with particular carbon number in the paraffin, naphthene, and aromatic, lumps. Fig. 3.7 is a representation of the yields of various iso-paraffins along the reactor. The trends reflect the production of paraffins at the beginning of the reactor until a maximum is reached and the consumption of those paraffins into lighter paraffins from the maximum to the end of the reactor. The initial increase in the yield of C_{33} can be

attributed to the rapid endocyclic cracking of C_{33} naphthenes. After the maximum, iso-paraffins in the residue fraction are further cracked to form lighter paraffins.

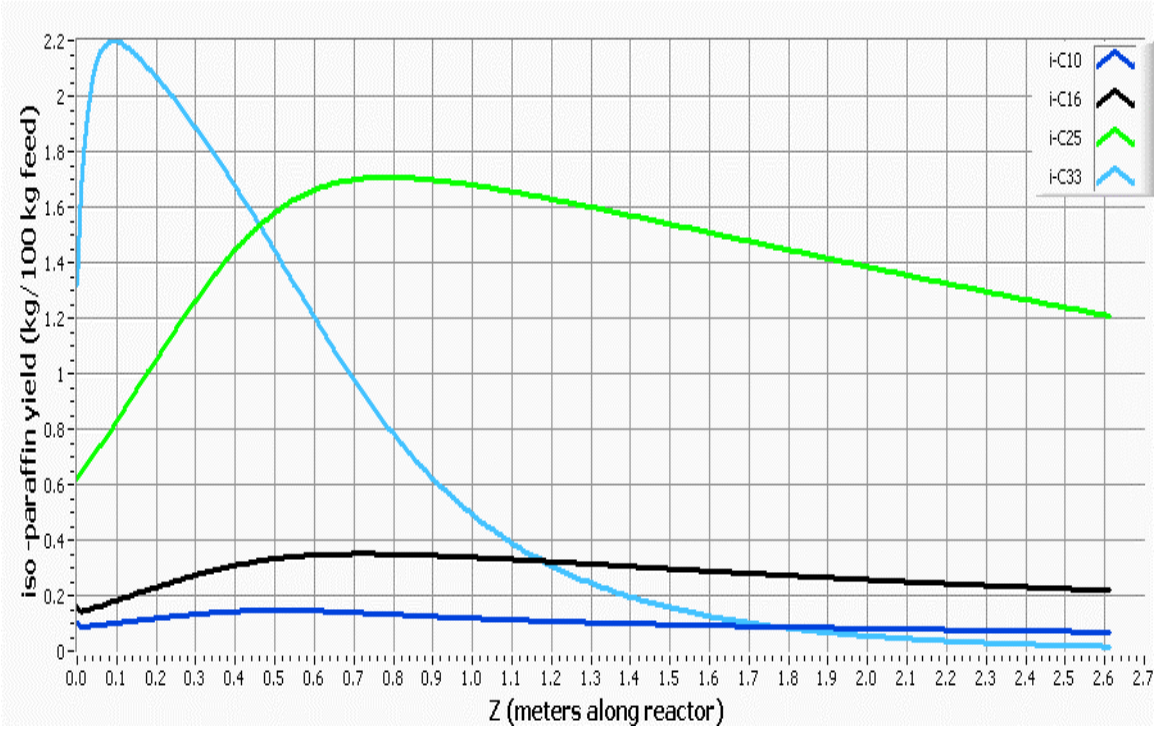

Fig. 3.7. Predicted Iso-Paraffin Yield

The feed composition and distribution of 1, 2, 3, 4-ring aromatics and naphthenes is shown in Table 3.8. The feed composition and distribution of 1, 2, 3, 4-ring naphtheno aromatics is shown in Table 3.9.

Table 3.8. Aromatic and Naphthene Feed Stream Characterization

%Aromatic [kg/100 kg feed]				**% Naphthene [kg/100 kg feed]**			
1-Ring	2-Ring	3-Ring	4-Ring	1-Ring	2-Ring	3-Ring	4-Ring
3.3%	2.6%	1.5%	1.0%	15.6%	13.9%	9.8%	3.2%
Wt% inlet aromatic [kg/kg aro]				**Wt % inlet naphthene [kg/kg naphthene]**			
1-Ring	2-Ring	3-Ring	4-Ring	1-Ring	2-Ring	3-Ring	4-Ring
39.3%	30.9%	17.7%	12.0%	36.8%	32.7%	23.1%	7.4%

Table 3.9. Naphtheno-Aromatics in Feed

% Naptheno-Aro [kg/100 kg feed]			
1-Ring	2-Ring	3-Ring	4-Ring
0.0%	6.7 %	7.3%	0.0%
Wt % of inlet naphtheno-aro [kg/kg]			
1-Ring	2-Ring	3-Ring	4-Ring
0.0%	47.9%	52.1%	0.0%

Table 3.10 and 3.11 shows the characterization of naphthenes and aromatics in the product stream as predicted by the model and from experiments conducted with an isothermal pilot reactor. By matching the corresponding colors of Table 3.9 and 3.10 a comparison can be made between the predicted and experimental yields of aromatics and naphthenes. The aromatic yields in Table 3.10 include the naphtheno aromatic fraction. Grouping naphtheno aromatics and aromatics provides a better comparison with experimental data provided. Mono-naphtheno aromatics and di-naphtheno mono-aromatics are lumped in with mono-aromatics in Table 3.10.

Table 3.10. Predicted Aromatic and Naphthene Product Stream Characterization

Aromatic % Yield [kg/100 kg feed]				**Naphthene % yield [kg/100 kg feed]**			
1-Ring	2-Ring	3-Ring	4-Ring	1-Ring	2-Ring	3-Ring	4-Ring
7.1%	4.9%	1.4%	0.9%	17.8%	14.2%	9.7%	3.2%
Wt% of exit aromatic [kg/kg aro]				**Wt % of exit naphthene [kg/kg naphthene]**			
1-Ring	2-Ring	3-Ring	4-Ring	1-Ring	2-Ring	3-Ring	4-Ring
49.7%	34.3%	9.7%	6.3%	39.6%	31.6%	21.6%	7.2%

Table 3.11. Experimental Aromatic and Naphthene Product Stream Characterization

Aromatic % Yield [kg/100 kg feed]				**Naphthene % yield [kg/100 kg feed]**			
1-Ring	2-Ring	3-Ring	4-Ring	1-Ring	2-Ring	3-Ring	4-Ring
2.3%	1.1%	1.0%	0.4%	22.8%	11.9%	9.0%	5.0%
Wt% of exit aro [kg/kg aro]				**Wt % of exit naphthene [kg/kg naphthene]**			
1-Ring	2-Ring	3-Ring	4-Ring	1-Ring	2-Ring	3-Ring	4-Ring
48.0%	23.0%	20.8%	8.2%	46.8%	24.4%	18.5%	10.3%

The predicted distribution of aromatics and naphthenes in the product stream predicted by the single-event model is in close agreement with the experimental product distribution of aromatics and naphthenes obtained from a pilot reactor. Table 3.12 shows the predicted and experimental yield of iso-paraffins and n-paraffins in the product stream. The predicted iso-paraffins are in close agreement with the experimental yield of iso-paraffins, and the predicted yield of n-paraffins is slightly low when compared to the experimental yield.

Table 3.12. Predicted and Experimental Isothermal Paraffin Yield

Paraffins	**Feed Wt % (kg/100 kg Feed)**	**Model Yield (kg/100 kg Feed)**	**Experimental Yield (kg/100 kg Feed)**
Iso	13.2%	33.1%	30.5%
Normal	20.4%	7.7%	16.0%

Table 3.13 includes the experimental and predicted yields of paraffins, naphthenes, and aromatics lumps in the product stream of the reactor. The naphtheno aromatic lump is combined with the aromatic lump in Table 3.13 for better comparison with experimental results.

Table 3.13. Total Isothermal Product Distribution [kg/100kg feed]

LUMP	**Model Yield**	**Experimental Yield**
Paraffin	40.8%	46.5%
Naphthene	45.0%	48.7%
Aromatic	14.2%	4.8%

The predicted yield of naphthene, paraffin, and aromatic lumps in the product stream are in relatively close agreement with the experimental results obtained from an isothermal pilot reactor.

The single-event model has the capability of predicting the evolution of components and lumps that are detailed to the carbon number. Further experimental data concerning the exit yield of particular lumps and components was obtained from an

industrial pilot reactor in order to realize the full capabilities of the model. Table 3.14 is showing the comparison of predicted and experimental exit yields of individual lumps and components within the paraffin and naphthene lumps.

Table 3.14. Yield of Components in Paraffin and Naphthene Lump [kg/100kg feed]

Experimental yield (fraction below 180 °C)			Model yield (fraction below 180 °C)		
Propane	0.00E+00		Propane	3.70E-03	
Isobutane	0.00E+00		Isobutane	3.24	
n-Butane	3.92E-02		n-Butane	2.60E-03	
Isopentane	1.04E-01		Isopentane	1.41E+00	
n-Pentane	3.97E-02		n-Pentane	2.50E-03	
Cyclopentane	4.02E-03		Cyclopentane	3.90E-04	
C6 Isoparaffins	1.70E-01		C6 Isoparaffins	1.41	
n-Hexane	4.26E-02		n-Hexane	1.40E-03	
Methylcyclopentane	8.88E-02	Sum C6	Methylcyclopentane		Sum C6
Cyclohexane	3.62E-02	1.25E-01	Cyclohexane		2.97E-01
C7 Isoparaffins	1.81E-01		C7 Isoparaffins	1.40E+00	
n-Heptane	3.43E-02		n-Heptane	2.48E-02	
C7 Cyclopentanes	1.55E-01	Sum C7	C7 Cyclopentanes		Sum C7
Methylcyclohexane	1.08E-01	2.63E-01	Methylcyclohexane		6.46E-01
C8 Isoparaffins	1.68E-01		C8 Isoparaffins	2.86E-01	
n-Octane	2.60E-02		n-Octane	4.07E-02	
C8 Cyclopentanes	1.42E-01	Sum C8	C8 Cyclopentanes		Sum C8
C8 Cyclohexanes	1.96E-01	3.38E-01	C8 Cyclohexanes		4.63E-01
C9 Naphthenes	3.16E-01		C9 Naphthenes	4.71E-01	
C9 Paraffins	1.80E-01		C9 Paraffins	4.09E-01	
C10 Naphthenes	2.21E-01		C10 Naphthenes	1.01E+00	
C10 Paraffins	1.67E-01		C10 Paraffins	3.86E-01	
C11 Naphthenes	3.92E-02		C11 Naphthenes	2.55E+00	
C11 Paraffins	5.10E-02		C11 Paraffins	6.83E-01	

The model has accurate predictions among the C_8-C_{11} paraffins and naphthenes, but some deficiencies do exist in the prediction of C_3-C_7 iso-paraffins. Further adjustments in the single-event parameters would provide better results among the C_3-C_7 iso-paraffins.

3.2 Simulation of Adiabatic Hydrocracking of HVGO

The following section includes the results of the adiabatic hydrocracking of partially hydrogenated vacuum gas oil. The single-event model was inserted into an adiabatic reactor model to obtain product distributions detailed to the carbon number, component, and lump. Industrial hydrocrackers are run adiabatically because multi-bed reactors are cheaper then an isothermal reactor with cooling tubes. The temperature is allowed to increase throughout each bed but not beyond temperatures that lead to undesired reactions. In this multi-bed adiabatic reactor the liquid effluent is cooled between each bed with hydrogen by cold shot cooling. The feed composition is the same as in the isothermal case and is described in Table 3.2. The operating conditions of the multi-bed adiabatic reactor are shown in Table 3.15.

Table 3.15. Adiabatic Operating Conditions

Reactor Type:	3-bed, 3 phase, adiabatic, tubular, trickle flow
Reactor Dimensions:	$\mathbf{\Omega} = 5.1*10^{-4}$ m^2; $\mathbf{z}$ = 2.63 m; $\mathbf{D}$ = 0.0254m
Inlet Pressure:	$\mathbf{P_i}$=160 bar
Inlet Temperature:	$\mathbf{T_r}$ = 335 ^{o}C
Liquid Molar Feed Rate:	$\mathbf{F} = 1.7*10^{-3}$ kmol/hr
Hydrogen/ Feed Molar Ratio:	γ = 30 kmol/kmol
Bulk Density of Catalyst:	ρ_B = 0.4155g/cc cat

The single-event frequency factor for the adiabatic simulation was obtained from the estimated isothermal single-event parameters at 350^o C. The appropriate Arrhenius and van't Hoff equations account for the temperature dependency of the single-event parameters.

The evolution of the various commercial petroleum fractions predicted by the model is shown in Fig. 3.8. The vertical bars in Fig 3.8 and following figures represent the end of a bed in the reactor. The third bed ends at 2.63 m and is not marked with a vertical bar. Within the residue fraction boiling above 370^o C, a 31.8% conversion is obtained, and significant amounts of LPG and LNAP are formed along the reactor as heavier feed components are converted. Table 3.16 shows the percent yield of each commercial fraction in the feed and at the exit of the reactor.

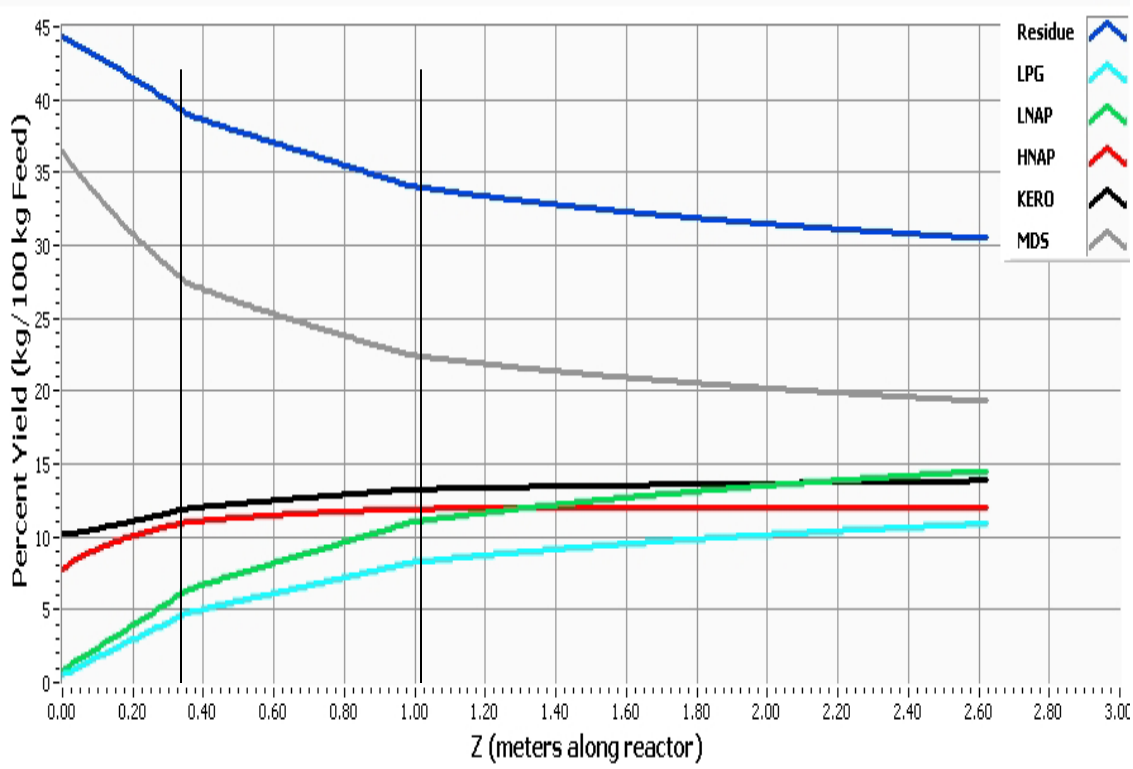

Fig. 3.8. Predicted Commercial Fractions in Adiabatic Operation

Table 3.16. Commercial Fractions in Adiabatic and Isothermal Operation

Model Predictions	**Yield [kg/100 kg feed]**	**Adiabatic Yield [kg/100 kg feed]**	**Isothermal Yield [kg/100 kg feed]**
Fraction	Feed	Product	Product
LPG (C_3-C_4)	0.5%	10.6%	11.9%
LNAP (C_5-C_7)	0.8%	14.4%	14.8%
HNAP (C_8-C_{12})	7.8%	11.8%	8.1%
KERO (C_{13}-C_{15})	10.2%	13.7%	9.8%
MDS (C_{16}-C_{24})	36.4%	19.3%	27.1%
Residue (> C_{24})	44.3%	30.2%	28.3%

Table 3.16 also shows a comparison of the yield commercial fractions yields in isothermal and adiabatic operations. The isothermal case shows higher conversions of residue and higher yields of LPG and MDS. The adiabatic case shows higher yields of KERO and HNAP. The range of products exiting adiabatic and isothermal reactors depends on the temperature evolution along the reactor in both reactors. The adiabatic

operation exhibited a range in temperature from 330-360^{o} C, and the isothermal reactor operated at 350^{o} C.

Fig. 3.9 shows the evolution of mono, di, tri, and tetra-naphthenes along the length of the 2.63 meter reactor. The di-naphthenes are rapidly formed in the first bed of the reactor due to the rapid hydrogenation and consumption of naphtheno mono-aromatics. The consumption of naphtheno-aromatics continues in the second bed of the reactor, where almost all naphtheno-aromatics are consumed. The hydrogenation and consumption of naphtheno di-aromatics and di-naphtheno mono-aromatics shown in Fig. 3.10, contributes to the generation of tri-naphthenes in the first and second bed of the reactor.

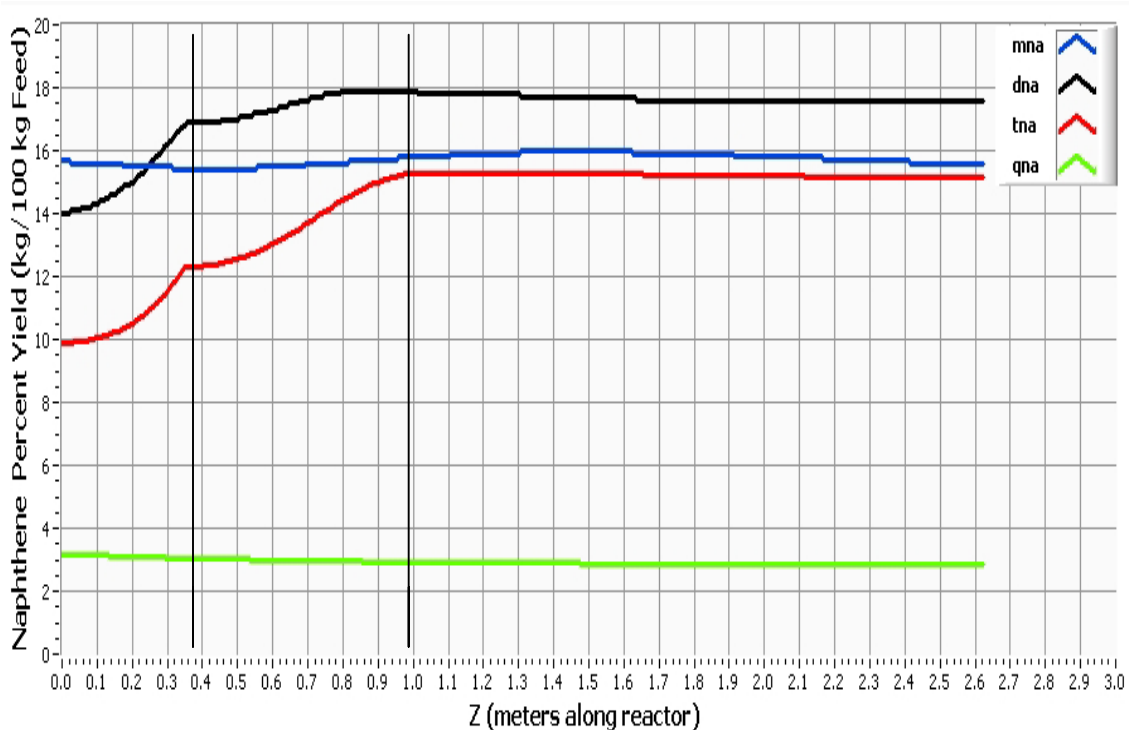

Fig. 3.9. Predicted Adiabatic Evolution of Naphthenes

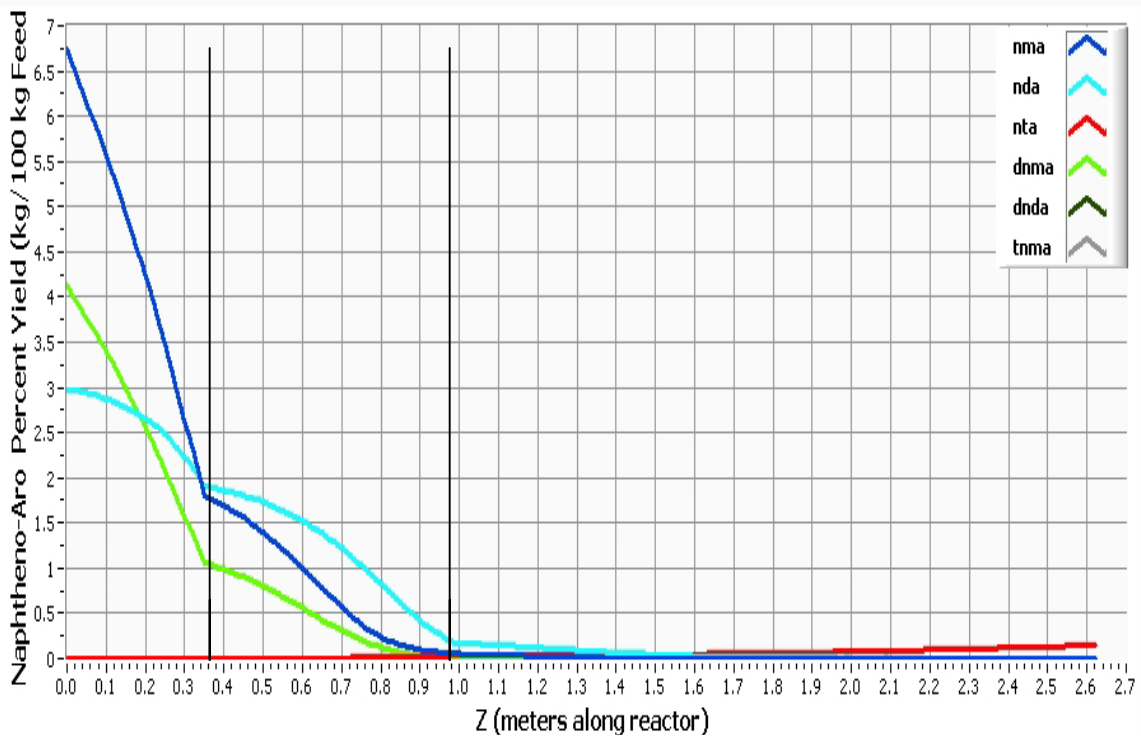

Fig. 3.10. Predicted Adiabatic Evolution of Naphtheno-Aromatics

Fig. 3.11 shows the evolution of aromatics in the axial direction of the reactor. The mono-aromatics are rapidly hydrogenated and converted into mono-naphthenes in beds 1 and 2 of the reactor. The rapid cracking of mono-naphthenes into paraffins accounts for the very low yield of mono-naphthenes. Di, tri, and tetra-aromatics are not as heavily hydrogenated as mono-aromatics and therefore do not contribute significantly to the formation of di, tri, and tetra-naphthenes respectively.

Fig. 3.12 illustrates the evolution of paraffins along the reactor. The rapid cracking of mono-naphthenes with straight side chains generates n-paraffins, which then undergo hydride shift, methyl shift, and PCP branching to generate iso-paraffins. The rapid cracking of mono-naphthenes with branched side chains contributes directly to the formation of iso-paraffins along the reactor.

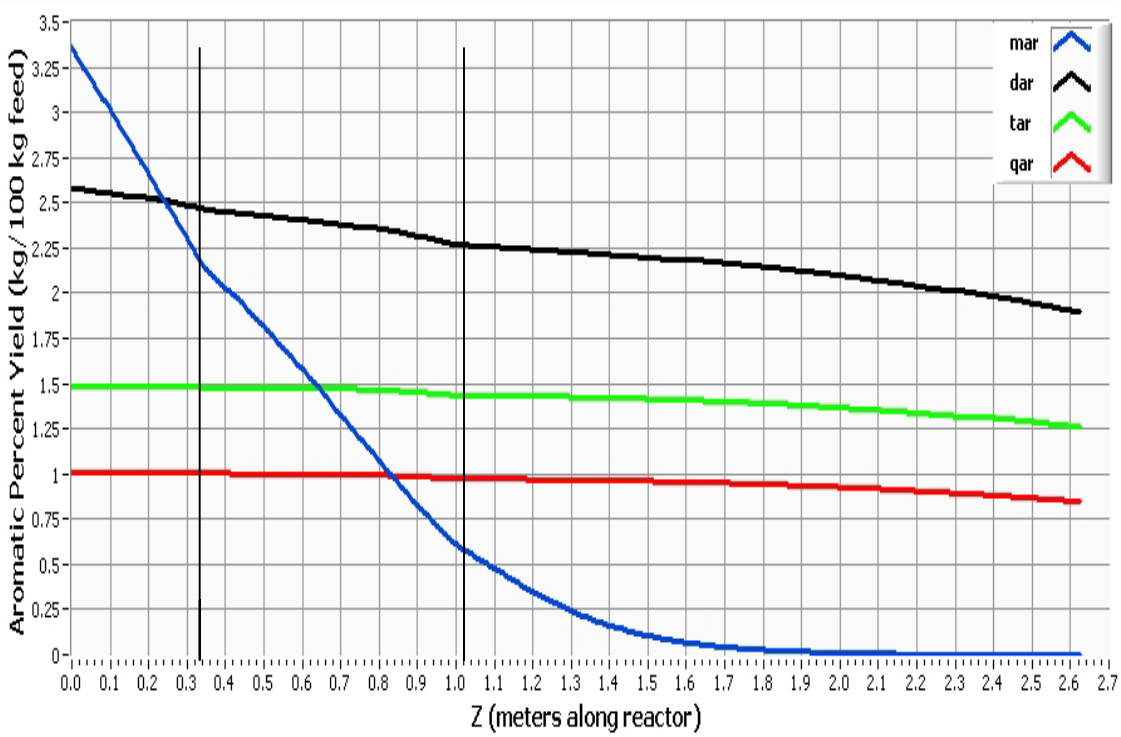

Fig.3.11. Predicted Adiabatic Evolution of Aromatics

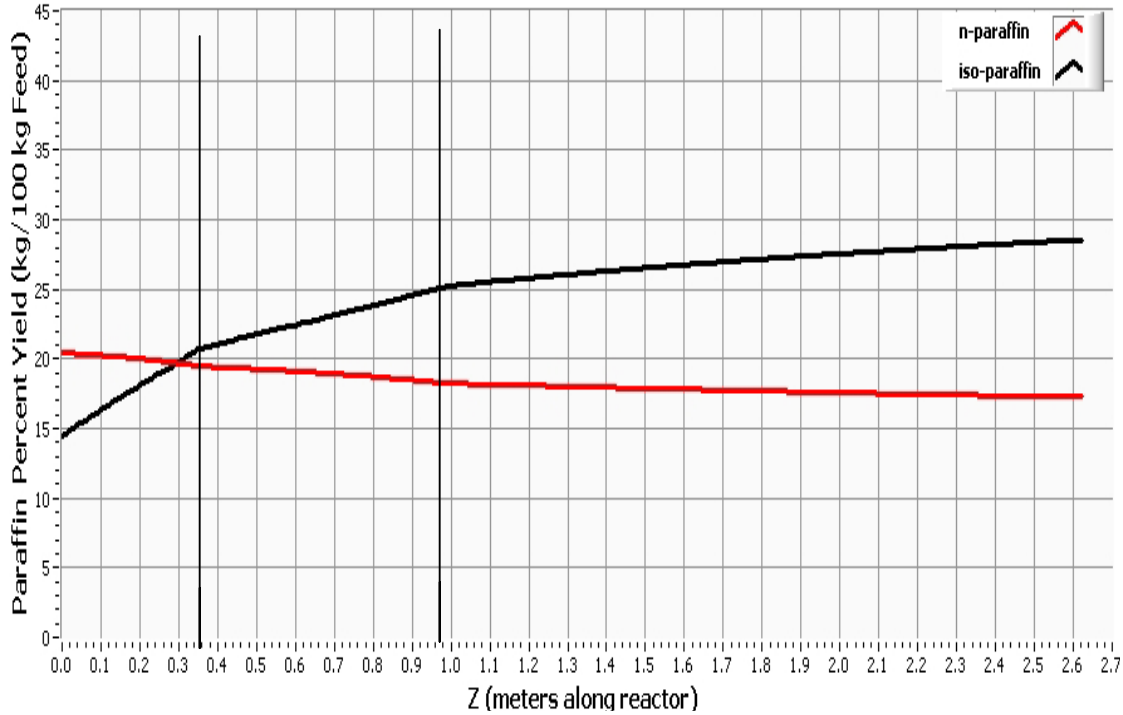

Fig. 3.12. Predicted Adiabatic Evolution of Paraffins

The hydrogen flux in both the gas and liquid phase is reported in units of [kmol/hr m^2 reactor] in Fig. 3.13. Hydrogen is consumed in the first bed of the reactor where rapid hydrogenation of aromatics occurs. Cold shot cooling by means of hydrogen (25^o C) after the first bed (0.36 m) increases the partial pressure of hydrogen in the gas phase which rapidly transfers hydrogen to the liquid phase. Hydrogen consumption continues through the second bed of the reactor, at the exit of the second bed (1 m), the hydrogen in the liquid phase increases due to rapid absorption of hydrogen from the gas to the liquid phase. Throughout the third bed of the reactor hydrogen is not significantly consumed, and due to high solubility of hydrogen in HVGO at 330^o C and greater, the hydrogen accumulates in the liquid phase. Cai et al (2001) determined the values of the solubility of hydrogen in HVGO. The amount of absorbed hydrogen in the liquid HVGO in the range of operating temperatures in this adiabatic process can be calculated using Fig 3.14.

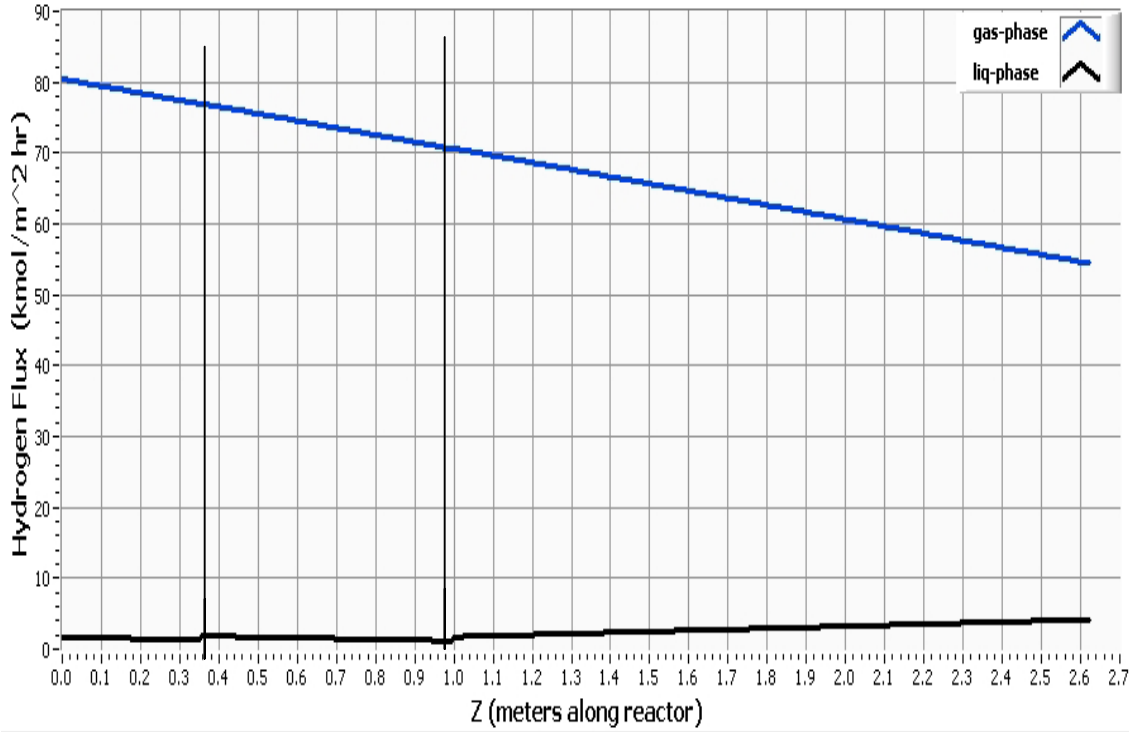

Fig. 3.13. Predicted Adiabatic Hydrogen Flux

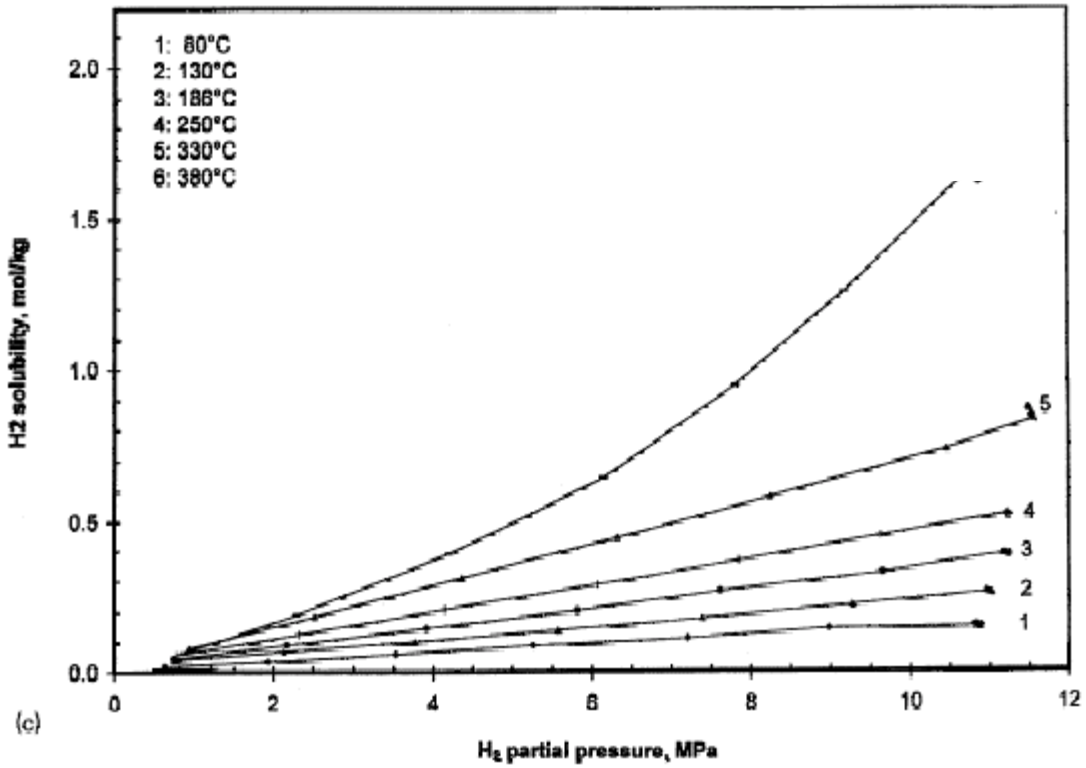

Fig 3.14 Solubility of Hydrogen in HVGO (Cai et al, 2001)

The partial pressure of hydrogen in the gas phase is 11.8 MPa, and the operating temperatures are between 335^{o} C and 365^{o} C as shown in Fig 3.15. Interpolation of hydrogen solubility lines in Fig 3.14 provides the solubility of gaseous hydrogen in liquid HVGO in moles of hydrogen per kilogram of liquid HVGO. The solubility of hydrogen in HVGO is between 1.2-1.6 mol/kg HVGO for the operating temperatures, and the hydrogen absorbed per unit area of reactor is between 1.2-1.6 kmol/hr m^2 for this adiabatic process.

Sharp increases in temperature can be observed through the first two beds of the reactor shown in Fig. 3.15. The reactions in hydrocracking are exothermic and the reactor temperature is expected to increase as the reaction progresses. The effluent is cooled to the inlet temperature (335^{o} C) after each bed as described in this section. A sharp increase in temperature is not exhibited in the third bed, because the most exothermic elementary steps occur in the first two beds, namely hydrogenation and cracking. There are minimal

differences in the solid, liquid, and gas phase temperature, which are calculated through correlations in section 2.5.

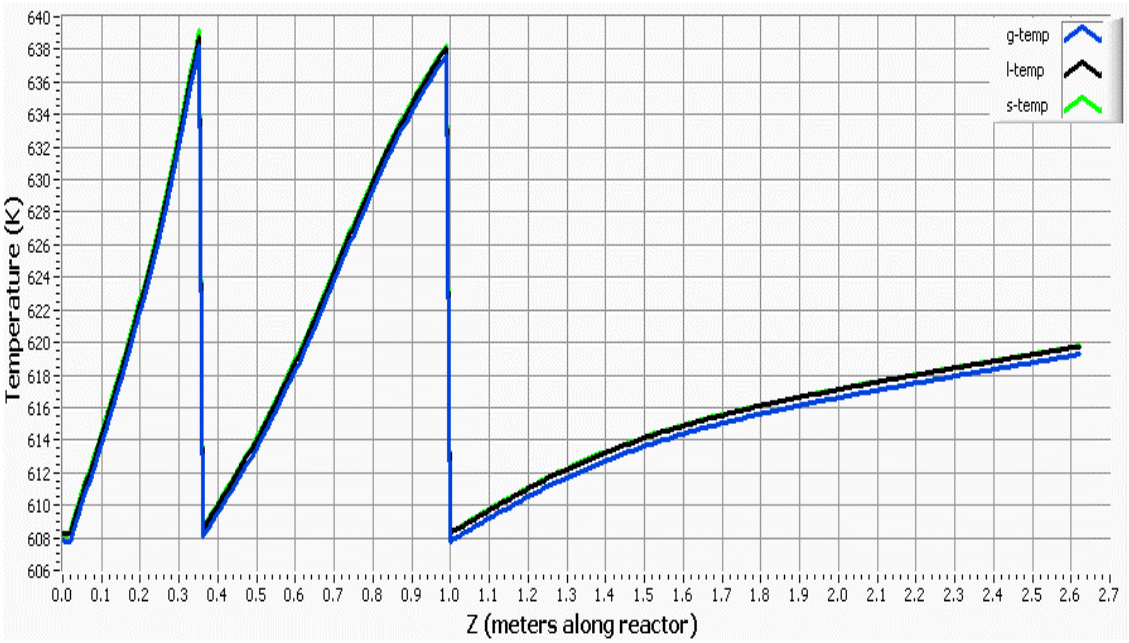

Fig. 3.15. Adiabatic Temperature Profile

Table 3.17 Total Product Yield in Adiabadic and Iosthermal Operation

Model Predictions	**Yield [kg/100 kg feed]**	**Adiabatic Yield [kg/100 kg feed]**	**Isothermal Yield [kg/100 kg feed]**
LUMP	Feed	Product	Product
paraffin	33.6%	45.8%	40.8%
naphthene	42.5%	51.1%	45.0%
aromatic	23.9%	3.1%	14.2%

Table 3.17 shows the total product distribution and feed composition in isothermal and adiabatic operations. The yields are in terms of paraffin, naphthene, and aromatic lumps. Aromatics are significantly consumed in reactions, contributing to an increase in naphthenes. A portion of the naphthenes that are produced from the hydrogenation of aromatics are cracked by β-scission to produce paraffins. A higher

amount of paraffins and naphthenes are produced in the adiabatic simulation as compared to the isothermal simulation due to a higher degree of aromatic hydrogenation and hydrogen consumption in adiabatic hydrocracking.

CHAPTER IV
SUMMARY AND CONCLUSIONS

It is apparent that the single-event model developed by Froment and coworkers can be applied to simulate the hydrocracking of HVGO in multi-phase, multi-bed, isothermal, and adiabatic operations. As a result of their fundamental formulation, the single-event parameters are invariant with respect to feedstock composition. This allows for feedstock or operating conditions used in industrial processes to be altered without losing the ability to efficiently predict product distributions. The temperature dependency of the single-event parameters and sorption parameters can be described through Arrhenius and van t Hoff's Law facilitating the estimation of parameters at any desired temperature

The single-event model has the ability to provide a wealth of information concerning the effect of operating conditions and feedstock composition on hydrocracker product distributions without having to conduct laboratory experiments. Furthermore, the model has the ability to predict the evolution of single components, lumps, fractions, temperature profiles, and hydrocracker hydrogen consumption throughout the reactor. The full potential of the fundamental model is realized when the operating conditions of an industrial hydrocracking process are optimized to provide product distributions which are high in demand in the current market.

To further develop the model, reactions involving sulfur, nitrogen, and oxygen that occur in the first stage of hydrocracking can be inserted into the model. Although catalyst deactivation is slow in the presence of high partial pressures of hydrogen a more complete model should include the alkylation reactions leading to coke formation that deactivates the catalyst. Hydrogenolysis reactions (cleavage by hydrogen), promoted by catalyst poisoning and responsible for producing methane and ethane, should also be inserted into the kinetic model.

NOTATION

$\widetilde{A}$	single-event frequency factor, kg cat/kmol·hr
C_{H^+}	surface concentration of vacant acid sites, kmol/kg cat
$C^*_{H^+}$	relative surface concentration of vacant acid sites w.r.t. total surface concentration of acid sites, kmol/kg cat
C_o, C_{ij}	olefin surface concentration, kmol/kg cat
C_{P_i}	paraffin surface concentration, kmol/kg cat
$C_{R_m^+}, C_{R_{ij,m}^+}$	carbenium ion surface concentration
$C^*_{R_m^+}, C^*_{R_{ij,m}^+}$	carbenium ion surface concentration, w.r.t. total surface concentration of acid sites, kmol/kg cat
$C_{s,sat}$	saturation surface concentration of sorbed hydrocarbons, kmol/kg cat
C_t	total surface concentration of acid sites, kmol/kg cat
D_{H_2G}	diffusivity of hydrogen from the gas to the liquid interface, m^2/s
D_{H_2L}	diffusivity of hydrogen from the liquid interface to bulk liquid, m^2/s
dar	di-aromatic
dna	di-naphthene
dnda	di-naphtheno-di-aromatic
dnma	di-naphtheno-mono-aromatic
E_a°	intrinsic activation barrier in EvansPolanyi relationship, kJ/kmol
h	planks constant 1.841 x 10^{-37}, J·h
H	Henry coefficient, m^3 bar/kmol
H^+	acid site
$\Delta H^{\circ\mp}$	standard activation enthalpy, kJ/kmol
ΔH_r	enthalpy of formation, kJ/kmol
ipa	iso-paraffin
k	rate coef. of elementary reaction

k'	single-event rate coef.
k_B	Boltzmann constant 1.381 x 10^{-31}, J/K
$k_{Pr}(m)$	rate coef. of protonation of an olefin to a carbenium ion of type m, kg cat/kmol·hr
$k_{De}(m;Oij)$	rate coef. of deprotonation of a carbenium ion m to olefin ij, h^{-1}
k_{H2G}	mass transfer coefficient of H_2 from gas to liquid interface, m/s
k_{H2L}	mass transfer coefficient of H_2 from liquid interface to bulk liquid, m/s
$k_{HS}(m;n)$	rate coef. of hydride shift between carbenium ions of type m and n, h^{-1}
$k_{MS}(m;n)$	rate coef. of methyl shift between carbenium ions of type m and n, h^{-1}
$k_{PCP}(m;n)$	rate coef. of PCP branching between carbenium ions of type m and n, h^{-1}
$k_{Cr}(m;n,O)$	rate coef. of cracking carbenium ion of type m into type and olefin O, h^{-1}
$k_H(ji)$	rate coef of hydrogenation of olefin ij to paraffin i, bar·hr^{-1}
$k_{DH}(ij)$	rate coef of dehydrogenation of paraffin i to olefin ij, h^{-1}
$K_{isom}(O_1 \Leftrightarrow O_2)$	equilibrium constant for olefin isomerization
$K_{D,H,ij}$	equilibrium constant for dehydrogenation of paraffin I to olefin ij, bar
$K_{L,i}$	Langmuir sorption equilibrium constant for hydrocarbon i, bar^{-1}
mar	mono-aromatic
mna	mono-naphthene
n_e	number of single events
N_{H2G}	molar flux of H_2 in gas phase, kmol/m^2s
N_{H2L}	molar flux of H_2 in liquid phase, kmol/m^2s
nda	naphtheno-di-aromatic
nma	naphtheno-mono-aromatic
npa	normal paraffin
nta	naphtheno-tri-aromatic
O	olefin
O_i	i^{th} olefin of reaction network
O_{ij}	olefin of structure i and double-bond j
p	partial pressure, bar
qar	tetra-aromatic

qna	tetra-naphthene
R_m^+	carbenium ion of type m
$R_{ij,m}^+$	carbenium ion of type m formed by protonation of olefin ij
R_{P_i}	net rate to paraffin formation, kmol/kg cat·hr
$R_{O_{ij}}$	net rate of formation of olefin ij, kmol/kg cat·
$R_{R_m^+}$	net rate of formation of carbenium ion m, kmol/kg cat·hr
s	secondary
S°	standard entropy kJ/kmol·K
$\Delta S^{\circ\mp}$	standard entropy of activation, kJ/kmol·K
t	tertiary
tar	tri-aromatic
tna	tri-naphthene
tnma	tri-naphtheno-mono-aromatic

Geek Letters

α	transfer coefficient
γ	hydrogen to hydrocarbon ratio
σ	symmetry number
σ_{gl}^r, $\sigma_{gl}^{\mp}$	global symmetry number for resp. reactant and transition state

Subscripts

Cr	cracking
De	deprotonation
Glob	accounting for symmetry and chirality
HS	hydrogen shift
HT	hydrogen transfer
i	interface

MS	methyl shift
PCP	PCP branching
Pr	protonation
r	reactant
‡	activated complex

REFERENCES

Alwahabi, S.M., & Froment, G.F., (2004). *Ind. Engng Chem. Res., 43*, 5098-5111.

Baltanas, M.A., & Froment, G.F. (1985). *Comput. Chem. Engng, 9*, 71-78.

Baltanas, M.A., Van Raemdonck, K.K., Froment, G.F., & Mohedas, R.S. (1989). *Ind. Engng Chem. Res*., *28*, 899-910.

Cai, H.Y., Shaw, J.M., & Chung K.H. (2001). *Fuel*, *80*, 1055-1063.

Froment, G.F., & Bischoff, K.B. (1990). *Chemical reactor analysis and design* (2nd ed.) New York: Wiley.

Gary, J. H., & Handwerk, G. E. (1984). *Petroleum refining technology and economics*. New York: Marcel Dekker Inc.

Gauw, F. J. M. M. (2002). Ph.D. Dissertation, *Kinetic studies of alkane hydroisomerization over solid acid catalysts,* Technische Universiteit Eindhoven, The Netherlands.

Krishna, R., & Saxena, A. K. (1989). *Chem. Engng Sci*., *44*, 703-712.

Kuznetsov P. N. (2003). *J. Catal*., *218*, 12-23.

Laximinarasimhan, C. S., Verma, R. P., & Ramachandran, P. A. (1996). *AIChE J*., *42*, 2645-2653.

Martens, G.G., Thybaut, J.W., & Marin, G.B. (2001). *Ind. Engng Chem. Res*., *40*, 1832-1844.

Moustafa, T. M., & Froment, G.F. (2003). *Ind. Engng Chem. Res., 42*, 14-25.

Park, T.Y., & Froment, G.F. (2001). *Ind. Engng Chem. Res*., *40*, 4187-4196.

Refining Flow Diagram. www.uop.com/refining/1010.html, 2004.

Scherzer, J., & Gruia, A. J. (1996). *Hydrocracking science and technolog.* New York: Marcel Dekker Inc

Schweitzer, J. M., Galtier, P., & Schweich, D. (1999). *Chem. Engng Sc*i., *54*, 2441-2452.

Strangeland, B. E. (1974). *Engng Chem. Proc. Des. Dev*., *13*, 71-76.

Treybal, R.E. (1980). *Mass transfer operations.* New York: McGraw Hill.

Vynckier, E., & Froment G.F. (1991). In G. Astarita & S.I. Sandler (Eds.), *Kinetic and thermodynamic lumping of multicomponent mixtures*.131-161. Amsterdam: Elsevier.

VITA

Alper T. Ertas was born March 20, 1979 in Bryan, Texas. He received a Bachelor of Science in chemical engineering from Texas A&M University in August of 2002. He studied in a biomedical engineering graduate program at The University of Texas in Austin. He joined the graduate program in chemical engineering at Texas A&M University in the fall of 2003, and graduated with a Master of Science in August 2005.

Alper T. Ertas
2918 N RR 620 #243
Austin, TX 78734